ELSEVIER

Tectonophysics 359 (2002) 329–358

TECTONOPHYSICS

www.elsevier.com/locate/tecto

Structure and kinematics of oblique continental convergence in northern Fiordland, New Zealand

Alexander L. Claypool[a], Keith A. Klepeis[a,*], Benjamin Dockrill[b], Geoffrey L. Clarke[b], Horst Zwingmann[c], Andrew Tulloch[d]

[a] *Department of Geology, University of Vermont, Burlington, VT 05405-0122, USA*
[b] *Division of Geology and Geophysics, School of Geosciences, University of Sydney, Sydney, NSW 2006, Australia*
[c] *CSIRO Petroleum, Technology Park, 3 Brodie Hall Drive, Bentley, WA 6102, Australia*
[d] *Institute for Geological and Nuclear Sciences, 764 Cumberland Street, Dunedin, New Zealand*

Received 22 August 2001; accepted 26 August 2002

Abstract

Southeast of the Alpine Fault in Fiordland, New Zealand, Late Tertiary faults envelope exposures of Early Cretaceous high-*P* (12–16 kbar) granulite facies orthogneisses. These exposures allowed us to examine how pre-Cenozoic structures influenced variations in the degree and style of kinematic partitioning within a zone of oblique continental convergence. Fault-slip data and kinematic modelling show that oblique-slip and reverse displacements preferentially were partitioned east of the Alpine Fault onto curved NE-striking surfaces and moderately dipping (30–52°), N- and NW-striking surfaces, respectively. Approximately 3.0–5.5 km of exhumation and 6.5–7.0 km of oblique-dextral displacement occurred on faults that display palm tree-style geometries and subhorizontal detachments in profile. This heterogeneous style contrasts with the near horizontal slip on subvertical surfaces that define the Alpine Fault north of Milford Sound. The principal axes of instantaneous strain we determined using faults are compatible with principal stress axes derived from earthquakes. Our data indicate that mechanical anisotropies created by inherited structures controlled the locations and highly variable geometries of faulting since 7–9 Ma. The effects of these pre-existing structures and a focusing of contractional deformation along the northeast margin of Fiordland resulted in an unusually high degree of strike-slip partitioning across the southernmost onshore segment of the Alpine Fault.

Keywords: Oblique convergence; Collisional tectonics; Transform plate boundary

1. Introduction

Zones of oblique plate convergence typically are characterized by deformation that is partitioned variably into orogen-parallel strike-slip faults, thrust and normal faults, and penetrative ductile fabrics. The South Island of New Zealand contains an active tectonic environment in which the current degree of strike-slip partitioning is low compared with other oblique orogens such as those in western North America (Mount and Suppe, 1987), Sumatra (McCaffrey, 1992), Eastern Turkey (Butler et al., 1998), and southern South America (Hervé, 1994). The low degree of strike-slip partitioning is indicated by virtually identi-

* Corresponding author. Tel.: +1-802-656-0246; fax: +1-802-656-0045.
E-mail address: kklepeis@zoo.uvm.edu (K.A. Klepeis).

0040-1951/02/$ - see front matter © 2002 Elsevier Science B.V. All rights reserved.
PII: S0040-1951(02)00532-2

cal oblique-reverse kinematics along many sections of an ~800 km continental transform called the Alpine Fault (Fig. 1) and in a broad zone of deformation 150–200 km wide east of this fault (Norris et al., 1990; Berryman et al., 1992; Norris and Cooper, 1995; Little, 1996). This style results from strong interplate coupling and the relatively high angle (~68°) of oblique convergence between the Australian and Pacific plates

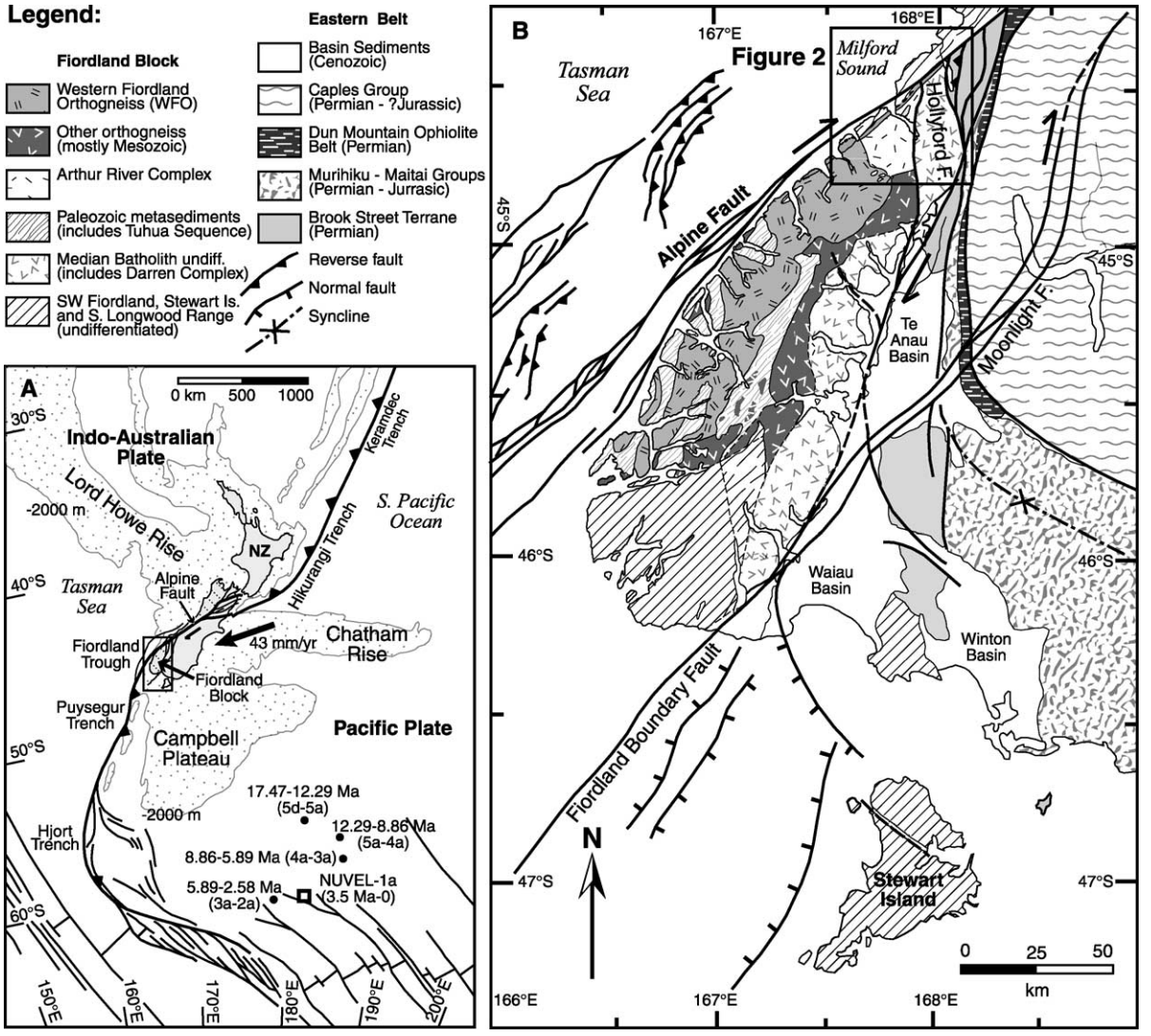

Fig. 1. (A) Tectonic setting of New Zealand. Indo-Australian–Pacific plate slip vector indicated (arrow). The Pacific plate has rotated counterclockwise relative to a fixed Australian plate about Euler poles (black dots) that have changed position with time (Walcott, 1998). Time periods and magnetic anomalies (in parentheses) for each pole of motion are indicated. The instantaneous, present-day Euler Pole (NUVEL-1a) is from DeMets et al. (1994). Inset shows location of the Fiordland region. (B) Map showing the geology and structure of the Fiordland Block and Eastern sedimentary belt. High-*P* granulites occur in the Arthur River Complex and Western Fiordland Orthogneiss. The Fiordland Block is outlined by the Alpine, Hollyford, Moonlight, and Fiordland Boundary faults (Norris and Carter, 1980; Norris and Turnbull, 1993). Offshore structures in the Tasman Sea are from Lebrun et al. (2000). Major lithologic divisions are from Bradshaw (1990).

since about 6.4 Ma (Koons, 1994; Braun and Beaumont, 1995; Teyssier et al., 1995; Walcott, 1998; Jiang et al., 2001).

Although Late Tertiary deformation in most of the Southern Alps involves strike-slip and dip-slip components, significant variations in the style and kinematics of deformation occur along the strike of the Alpine Fault. The Fiordland region (Fig. 1) in particular contains several unusual features. First, surface deformation along the southernmost onshore segment of the Alpine Fault involves almost pure strike-slip displacement on near vertical surfaces (Sutherland and Norris, 1995; Norris and Cooper, 2001). In contrast, surface deformation along other segments of the Alpine Fault farther north involves oblique-thrust motion on moderately (~ 30°) ESE-dipping fault segments and dextral strike-slip motion on ENE-striking subvertical segments (Norris et al., 1990; Norris and Cooper, 1995). These data suggest that the degree of kinematic partitioning between slip on the Alpine Fault and deformation east of the fault is higher near Fiordland than it is along fault segments located farther north.

A second unusual feature is that Fiordland contains over 5000 km^2 of exhumed Early Cretaceous high pressure (P=12–16 kbar) granulite facies orthogneisses (Blattner, 1976; Oliver and Coggon, 1979; Gibson et al., 1988; Bradshaw, 1989; Clarke et al., 2000). New Zealand rocks representative of these unusually deep (>45 km) paleodepths are unique to Fiordland. Previous work suggests that the high-pressure granulites were exhumed to depths of ~ 10 km in the mid-Cretaceous (Mattinson et al., 1986; Nathan et al., 2000; Davids and Gibson, 2001) and later from depths of ~ 10 km to surface levels in the Late Tertiary (Sutherland, 1996). The pre-Cenozoic architecture of the Fiordland crust likely influenced both the mechanism of exhumation and the geometry of late Cenozoic deformation (Blattner, 1991; Klepeis et al., 1999; Sutherland et al., 2000; Lebrun et al., 2000). However, the specific effects of Tertiary strike-slip, oblique-slip and contractional deformation on the evolution of these granulites, including their exhumation, are unclear. Most of the shortening that occurs normal to the Alpine Fault may be accommodated east of the granulites (Walcott, 1998). Nevertheless, Blattner (1991) identified a series of brittle faults and steep amphibolite facies foliations in the northern part of the granulite belt that he interpreted as the exhumed roots of a zone of transpression. Hill (1995) inferred that Late Tertiary deformation affecting the granulites was dominated by a >10-km wavelength antiform. Norris and Turnbull (1993) suggested that Miocene oblique-slip and reverse faults northeast of the granulite belt were linked to the northward displacement and uplift of Fiordland crust.

In this paper, we present structural, kinematic and preliminary geochronologic data from the Fiordland granulite belt southeast of the Alpine Fault and north of Milford Sound (Figs. 2 and 3). Excellent exposure and well defined boundaries allowed us to investigate how strike-slip, oblique-slip and contractional styles of deformation were partitioned within and at the edges of this granulite belt. Distinctive metamorphic mineral assemblages and good crosscutting relationships enabled us to establish how Late Tertiary deformation of variable geometry and kinematic significance are related to older structures. Fault-slip and kinematic data show that approximately 6.5–7.0 km oblique-slip and reverse slip were partitioned onto surfaces of variable orientation. Fault zones up to 2 km wide display curved palm tree-style fault sets underlain by subhorizontal detachments. This segmented style is comparable to some parts of the Alpine Fault located farther north, except that in Fiordland it has been transferred tens of kilometers to the east of the Alpine Fault. We conclude that the high degree of strike-slip partitioning in northern Fiordland and its wedge-shaped, fault-bounded structure reflect an inherited crustal architecture that controlled the location, geometry, and kinematics of Tertiary deformation.

2. Geologic history and tectonic setting of the granulite belt

Gabbroic to dioritic orthogneisses and metasediments of the Fiordland Block (Fig. 1B) record a history of Paleozoic and Early Cretaceous orogenesis. Paleozoic tectonism involved contractional deformation, low- to high-grade metamorphism, and pluton emplacement within the Pacific margin of Gondwana from ~ 481 to ~ 334 Ma (Oliver, 1980; Gibson et al., 1988; Ireland and Gibson, 1998). Crustal thickening and tectonic burial during this

period are indicated by medium to high pressure ($P=7-9$ kbar) kyanite-bearing assemblages that overprint lower pressure ($P=3-5$ kbar) sillimanite-bearing assemblages in Paleozoic metasediments (Gibson, 1990).

Superimposed on Paleozoic events is a record of Early Cretaceous arc-related pluton emplacement, high-P upper amphibolite–granulite facies metamorphism, and intense contractional deformation (Bradshaw, 1989; Oliver, 1990; Brown, 1996; Gibson and Ireland, 1995). These events coincided with the emplacement of a major calc-alkaline batholith and the accretion of outboard terranes onto the Pacific margin of Gondwana (Mattinson et al., 1986; McCulloch et al., 1987; Tulloch and Kimbrough, 1989; Mortimer et al., 1999). Most of the accreted terranes now make up the Eastern Belt of SW New Zealand (Fig. 1B). In northern Fiordland (Figs. 2 and 3), the batholith includes 126–119 Ma metadiorite and metagabbro of the Western Fiordland Orthogneiss (WFO, Fig. 1B) and leucogabbro and diorite of the 141–137 Ma Darran Complex (Bradshaw, 1990; Kimbrough et al., 1994; Mortimer et al., 1999). The Western Fiordland Orthogneiss intruded the Arthur River Complex (Mattinson et al., 1986; Bradshaw, 1990). U–Pb ion probe dates on zircons from the Arthur River complex yielded some Paleozoic protolith ages (355 ± 10 Ma) and metamorphic ages at ~ 134 and ~ 120 Ma (Tulloch et al., 2000). Garnet–pyroxene–plagioclase-bearing assemblages within the Arthur River Complex and the Western Fiordland Orthogneiss give metamorphic pressures ($P=12-16$ kbar) indicative of lower crustal paleodepths (Blattner, 1978; Bradshaw, 1989; Clarke et al., 2000; Daczko et al., 2001).

By 108–105 Ma extension affected parts of the Fiordland belt and adjacent areas (Bradshaw, 1989; Tulloch and Kimbrough, 1989; Gibson and Ireland, 1995). The Doubtful Sound shear zone located in central Fiordland formed during this period (Gibson et al., 1988; Gibson and Ireland, 1995). In northern Fiordland, the Anita Shear Zone (Fig. 2) contains several superposed fabrics that formed during or after this period (Hill, 1995; Klepeis et al., 1999; Nathan et al., 2000). $^{40}K-^{39}Ar$ ages of hornblende (Nathan et al., 2000) and U–Pb dates of apatite (Mattinson et al., 1986) suggest that the granulites had cooled to 300–400 °C by ~ 90 Ma.

Late Cretaceous extensional and rifting associated with the breakup of Gondwana led to the opening of the Tasman Sea basin between Australia and New Zealand by ~ 84 Ma (Gaina et al., 1998). By approximately 52 Ma, sea floor spreading along the central Tasman ridge system had ended (Gaina et al., 1998) and a new period of rifting initiated in the southwest Tasman Sea region south of New Zealand (Weissel et al., 1977). Here, the Pacific–Australia plate boundary developed as a spreading center at least by 47–45 Ma (Sutherland et al., 2000). From 30 to 11 Ma, the spreading direction became progressively more oblique and the boundary eventually evolved into a transform as the relative pole of rotation between the Pacific and Australian plates migrated southward (Lamarche et al., 1997). Spreading ceased and oblique subduction initiated beneath the continent between 12 and 10 Ma (Davey and Smith, 1983). Later, clockwise rotation of the Euler pole (Fig. 1A) resulted in strike-slip motion along most of the plate boundary, followed by transpression (Sutherland, 1995). Near the end of the Miocene (~ 6.4 Ma), a decrease in the obliquity of plate convergence resulted in an increase in the rate of convergence and the uplift of the Southern Alps (Walcott, 1998).

Approximately 70–75% of motion arising from the current regime of oblique convergence between the Australian and Pacific plates is accommodated by orogen-parallel slip along the Alpine Fault (Sutherland et al., 2000; Norris and Cooper, 2001). This fault links the E-dipping Puysegur trench to the south with the west-dipping Hikurangi subduction zone to the north (Fig. 1A). Four hundred and sixty kilometers of offset have accumulated along the Alpine Fault (Wellman, 1953). Uplift rates are estimated at 5–12 mm/year (Bull and Cooper, 1986; Walcott, 1998). Plate motion vectors near the central section of the Southern

Fig. 2. (a) Geologic map of northern Fiordland showing main rock units and faults. Geology is based on mapping completed for this study and Wood (1962, 1972), Norris and Carter (1980, 1982), Landis (1980), Coombs and Landis (1985), Bradshaw (1990), Blattner (1991), Norris and Turnbull (1993), Sutherland (1994), Sutherland and Norris (1995), Klepeis et al. (1999); and Clarke et al. (2000). (b) Cross section (no vertical exaggeration) showing orientations of faults and foliation traces were constructed using data from this study. Fault trace locations are constrained with digital terrain data.

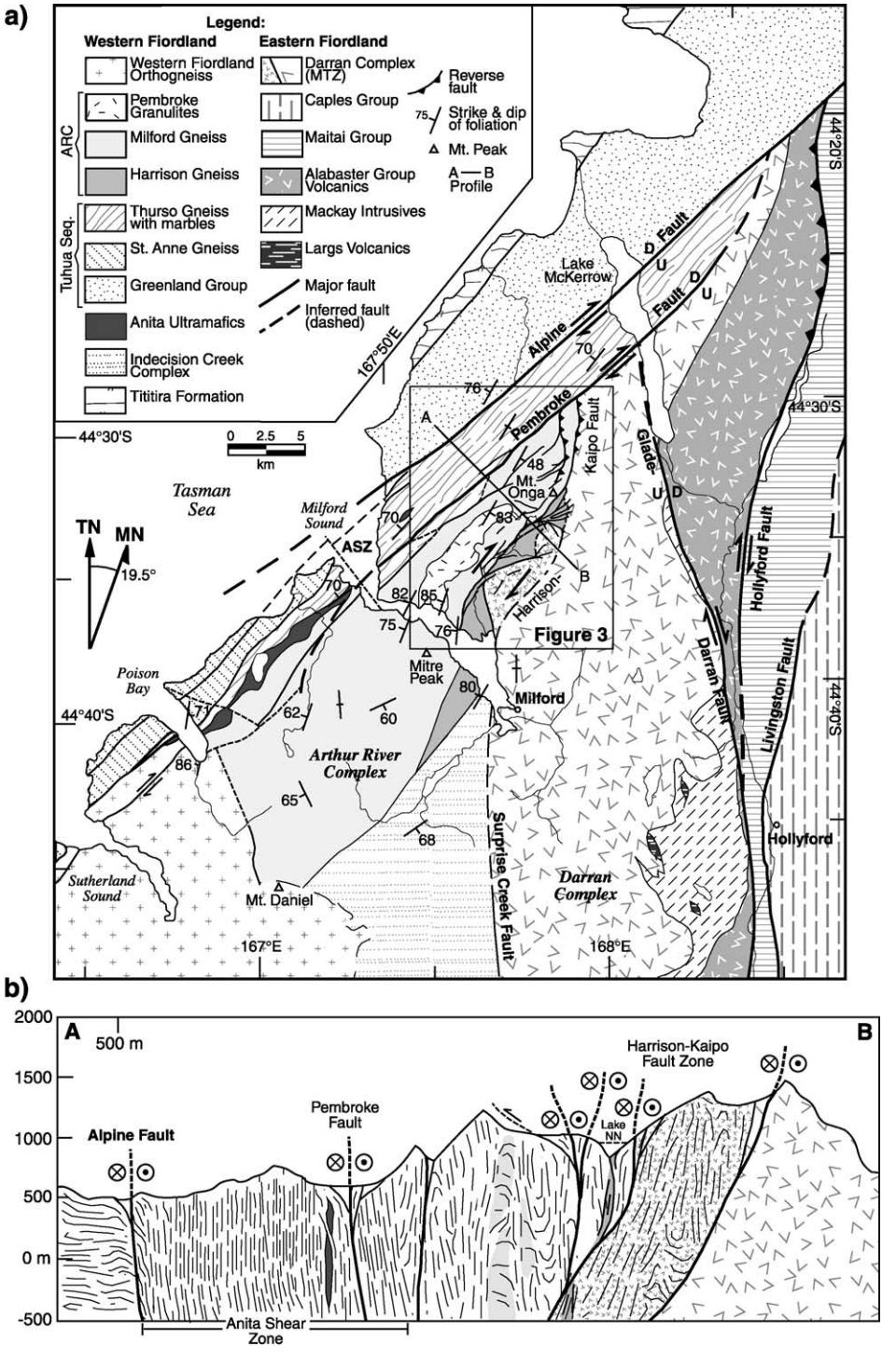
a)
Legend:
Western Fiordland
Eastern Fiordland
Western Fiordland Orthogneiss
Pembroke Granulites
Milford Gneiss
Harrison Gneiss
Thurso Gneiss with marbles
St. Anne Gneiss
Greenland Group
Anita Ultramafics
Indecision Creek Complex
Tititira Formation
ARC
Tuhua Seq.
Darran Complex (MTZ)
Caples Group
Maitai Group
Alabaster Group Volcanics
Mackay Intrusives
Largs Volcanics
Major fault
Inferred fault (dashed)
Reverse fault
Strike & dip of foliation
Mt. Peak
A — B Profile
44°20'S
44°30'S
44°40'S
167°50'E
168°E
167°E
0 2.5 5
km
Tasman Sea
Milford Sound
TN
MN
19.5°
ASZ
Lake McKerrow
D Fault
U
Fault
Alpine
Pembroke
Kaipo Fault
Glade
Mt. Onga
Harrison-
Figure 3
Hollyford Fault
Livingston Fault
Darran Fault
Mitre Peak
Milford
Hollyford
Poison Bay
Arthur River Complex
Surprise Creek Fault
Darran Complex
Sutherland Sound
Mt. Daniel
b)
A
B
500 m
2000
1500
1000
500
0 m
-500
Alpine Fault
Pembroke Fault
Harrison-Kaipo Fault Zone
Lake NN
Anita Shear Zone

Alps have been calculated from global plate models at rates of 39–45 mm/year at azimuths of 071–083° (Chase, 1978; Walcott, 1979, 1998; DeMets et al., 1994). Late Quaternary slip rates indicate that 27 ± 5 mm/year of strike-slip occurs on the Alpine Fault north of Milford Sound (Sutherland, 1994). Dip-slip rates show variation along strike of the Alpine Fault with a maximum of >10 mm/year in the central section and decreasing to zero near Milford Sound (Norris and Cooper, 2001). These estimates imply late Quaternary rates of shortening as high as 25 ± 3 mm/year may be accommodated away from the southernmost (onshore) segment of the Alpine Fault. Other estimates suggest shortening rates across the Alpine Fault range from 10 to 16 mm/year (Walcott, 1998).

3. Structure of northern Fiordland

In this section, we describe the structure and metamorphic characteristics of the Arthur River Complex near Milford Sound (Figs. 2 and 3), including its boundaries. We also discuss crosscutting relationships that enabled us to determine a sequence of deformation and metamorphism.

3.1. The Arthur River Complex and its boundaries

Upper amphibolite and granulite facies orthogneisses of the Arthur River Complex (Fig. 2) may be subdivided into mafic units including the Milford Gneiss and Pembroke Granulite, and the metadioritic Harrison Gneiss (Wood, 1972; Blattner, 1991). The Harrison Gneiss contains discontinuous bands of mafic to felsic compositions in gradational and, locally, faulted contact with subvertical sheets of mafic Milford Gneiss. The Pembroke Granulite includes two-pyroxene, hornblende-bearing metagabbros that occur as low strain lenses within the Milford Gneiss (Fig. 2). All contacts between these units parallel a regionally penetrative, vertical to steeply dipping, Early Cretaceous gneissic foliation that strikes to the NNE and dips variably to the NW and SE (Figs. 2b and 3). The low strain lenses of the Pembroke Granulite preserve evidence for deformation, also of Early Cretaceous age, that slightly predate the main foliation mapped throughout the rest of the Arthur River Complex (Clarke et al., 2000; Daczko et al., 2001). The fabrics in these lenses have been related to contraction of the Early Cretaceous orogen and loading of the granulites from $P<8$ kbar to $P=12–14$ kbar (Clarke et al., 2000; Daczko et al., 2001). They include granulite facies garnet–clinopyroxene-bearing reactions zones within gabbroic and dioritic plutons that are deformed by steep sinistral shear zones and vertically stacked ductile thrust faults (Daczko et al., 2001). For the purpose of this paper, we refer to the dominant Early Cretaceous fabric in the Arthur River Complex as S_1 because all of the Tertiary structures discussed herein cut this foliation.

S_1 is defined by flattened clusters of hornblende, garnet, plagioclase, clinozoisite and rutile, with or without clinopyroxene, paragonite, phengitic white mica and biotite. Steeply plunging, down-dip amphibole and plagioclase mineral lineations (L_1) occur on foliation planes (Fig. 3). Average $P–T$ calculation methods and directly calibrated geobarometers used on S_1 assemblages produced estimates of maximum metamorphic pressures of 10–14 kbar (Clarke et al., 2000).

The dominant $L_1–S_1$ fabric is cut by a series of fault zones that form a wedge shape along the margins of the Arthur River Complex north of Milford Sound. The western boundary of this wedge coincides with the eastern boundary of the Anita Shear Zone (Figs. 2 and 3). This shear zone has vertical boundaries that strike to the NE, parallel to the Alpine and Pembroke faults. At least two generations of upper amphibolite facies mylonitic fabrics occur within the shear zone, both of which cut $L_1–S_1$ in the Arthur River Complex (Klepeis et al., 1999).

The Anita Shear Zone is cut by ductile upper greenschist facies shear zones and brittle faults that are localized at its boundaries. The upper greenschist facies shear zones contain vertical mylonitic foliations defined by flattened clusters of phengitic white mica, chlorite, biotite and recrystallized quartz. South of Milford Sound, the main trace of the Alpine Fault diverges offshore and west of the Anita Shear Zone. Here, splays of the Alpine and Pembroke faults reactivate both sides of the Anita Shear Zone (Fig. 2).

The eastern boundary of the Arthur River Complex north of Milford Sound is defined by a 2-km-wide fault zone that we name the Harrison–Kaipo fault zone (after Blattner, 1991). This fault zone (Figs. 2 and 3) contains vertical to moderately NW-dipping en

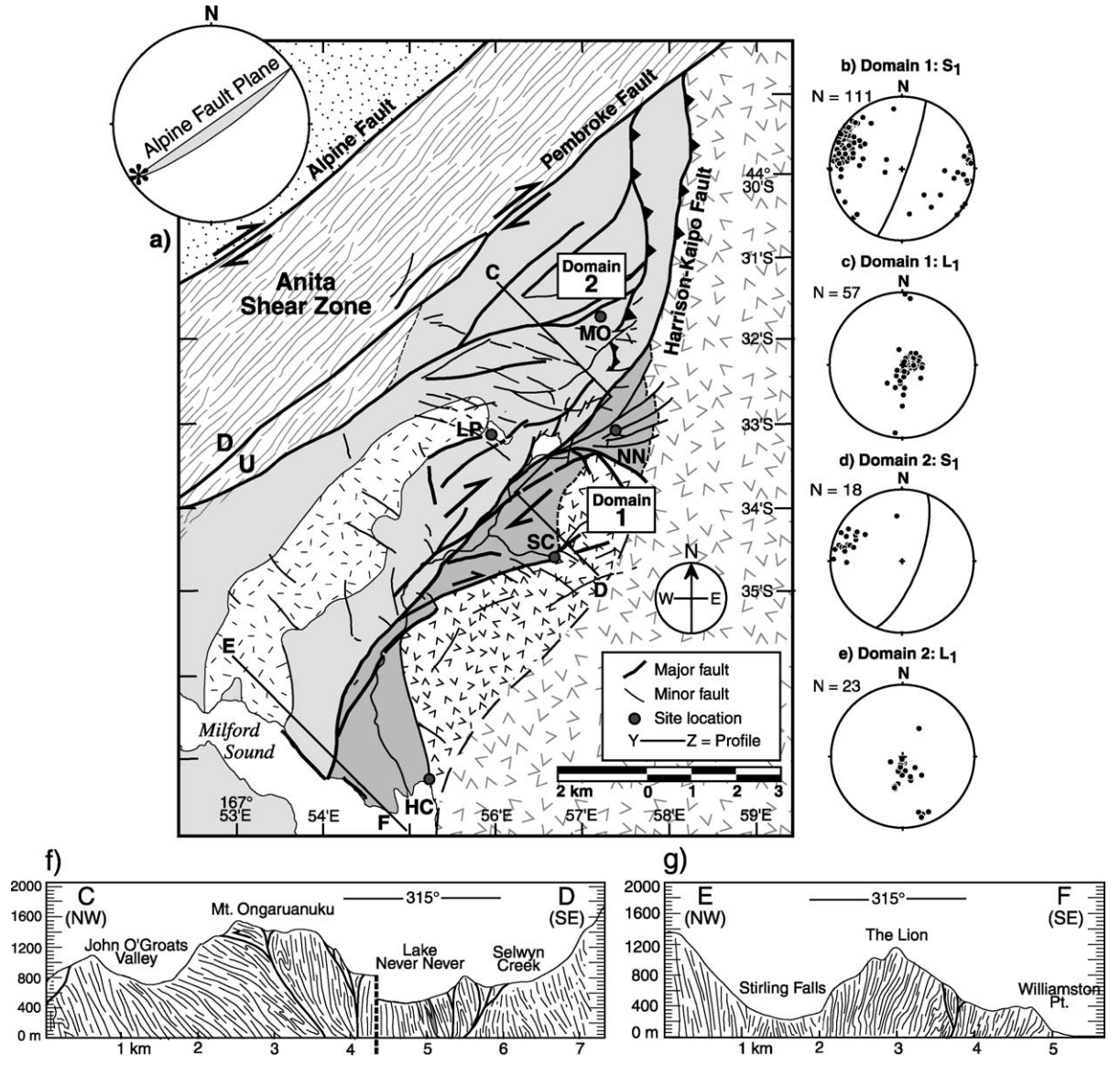

Fig. 3. (a) Geologic map of the Alpine, Pembroke and Harrison–Kaipo fault zones north of Milford Sound. Geologic units same as in Fig. 2. Unit shown by pattern of closely spaced triangles east of Selwyn Creek (SC) is composed of hornblende diorite and garnet–biotite gneiss intruded by dikes and is the newly identified unit discussed in the text. Bold black lines are major faults, thin black lines are minor fault traces, dashed lines are inferred fault. Lower hemisphere, equal-area stereoplot (top-left) shows orientation of Alpine Fault striking 055° and dipping 80° SE. Asterisks (*) shows near horizontal slip (from Sutherland and Norris, 1995). (b–e) Lower hemisphere equal area stereoplots showing foliations (S_1) and hornblende mineral lineations (L_1) from structural domains 1 and 2. See text for description of domains. Site locations: MO is Mt. Ongaruanuku, NN is Never Never Valley, LP is Lake Pukutahi, SC is Selwyn Creek, and HC is Harrison Cove. (f–g) Cross sections showing orientations of S_1 foliation traces. No vertical exaggeration. Vertical dashed line in (f) is the break in the cross section indicated in (a).

echelon faults, tight, variably plunging folds, and upper greenschist facies shear zones that deform the Harrison Gneiss and separate it from rock units to the east. South of Milford Sound, the Harrison Gneiss–Darran contact is reported as gradational in some areas (Blattner, 1991) and defined by the Surprise

Creek fault in others (Koons, 1978; Tulloch et al., 2000). One area where a gradational contact may be preserved is at Harrison Cove (HC, Fig. 3) (Hollis, 1996; Clarke et al., 2000) where splays of the Harrison–Kaipo fault zone cut southwest and away from the Darran Complex. Thirty-three kilometers northeast of Milford Sound, the Harrison–Kaipo fault curves and abuts against the Pembroke fault.

3.2. Structures east of the Arthur River Complex

East of the Harrison–Kaipo fault zone is a narrow, 1–2 km wide unit composed of hornblende diorites and garnet–biotite gneiss intruded by amphibolitic to felsic dikes (Fig. 3). At Selwyn Creek (SC; Fig. 3) many of these dikes are discordant to a steep amphibolite facies foliation that parallels S_1 in the adjacent Arthur River Complex. Within this unit, an S_1 assemblage of garnet–hornblende–bioite–plagioclase–clinozoisite–paragonite–quartz yielded estimates of the peak of metamorphism at $P = 11–13$ kbar, $T = 560–650$ °C (Dockrill, 2000). These high-grade conditions are inconsistent with the weakly metamorphosed character of most of the Darran Complex (Wandres et al., 1998). The presence of highly discordant dikes, magmatic flow foliations, and the syntectonic partial melting of dioritic host rocks also distinguish this unit from the Harrison Gneiss (Fig. 2). We suggest that these rocks represent either a deformed and metamorphosed part of the Darran Suite of Muir et al. (1995, 1998) or a northern equivalent of the Early Cretaceous Indecision Creek Complex of Bradshaw (1990).

East of this unit are weakly deformed and unmetamorphosed diorite of the Darran Complex (Bradshaw, 1990; Wandres et al., 1998; Tulloch et al., 2000). The Glade–Darran fault coincides with the eastern contact of the Darran Complex NE of Milford Sound but diverges into the Mackay Intrusives at its southern end (Fig. 2). This fault strikes to the NNW and terminates against the Pembroke fault 10 km north of the Harrison–Kaipo–Pembroke intersection. To the south, it connects with N- and NNE-striking segments of the Moonlight and Fiordland Boundary faults (Fig. 1). The curved geometry of the Glade–Darran–Moonlight fault system is identical to that displayed by the Harrison–Kaipo fault. The Hollyford and Livingston faults also occur east of the Darran Complex (Fig. 2). These faults are curved, containing N- and NE-striking segments that merge with the Glade–Darran fault southeast of Milford Sound. The Hollyford fault abuts against the Alpine Fault ~ 16 km northeast of the Glade–Darran–Pembroke fault intersection.

4. The Harrison–Kaipo and Pembroke fault zones

In this section, we present data on fault-related structures, ductile shear zones, and folds in the Harrison–Kaipo and Pembroke fault zones north of Milford Sound (Fig. 3). Two domains display distinctive patterns. Domain 1 includes structures located between the Darran Complex and the Pembroke Fault from Milford Sound to Lake Never Never (NN, Fig. 3). Localities within this domain include Lake Pukutahi, Selwyn Creek, Lake Never Never, Pembroke Valley, and the Harrison Valley. Domain 2 includes exposures at and near the intersection between the Harrison–Kaipo fault and the Pembroke fault surrounding and north of Mount Ongaruanuku (MO, Fig. 3).

4.1. Domain 1: strike-slip faults and related structures

Domain 1 contains two mutually crosscutting fault populations (Figs. 4 and 5) that are distinguishable on the basis of strike orientation, trace length, magnitude of displacement, and sense of displacement. Faults in the first population are the largest, displaying traces up to 15 km long although they more typically are

Fig. 4. (a) Sketch of vertical cliff wall at site NN in Fig. 3a (horizontal distance is ~ 1 km). View is to the NE, perpendicular to the 049° strike of the main traces of the Harrison–Kaipo fault zone. Sketch shows curved oblique-slip fault segments (thick lines) that form palm tree-style structures in profile. Foliation planes (thin lines) dip to the SE and are folded. Arrow shows creek bed used to construct (b) and (c). (b) Vertical cross section showing fault geometry in the zone in an incised creek bed. Fault traces (thick lines), folded S_1 foliation planes (thin lines), and faulted dikes (white) are shown. Note apparent subhorizontal detachments below steep branching oblique-slip faults. Sense of shear along subvertical faults is both sinistral and dextral. The flat lying detachment faults show an apparent oblique-thrust sense. (c) Form map of creek bed below (b) showing asymmetric lenses of Harrison Gneiss enveloped by oblique-slip faults. For both (b) and (c), fault trends for dextral and sinistral fault sets are given in Fig. 10a and e, respectively. See text for discussion.

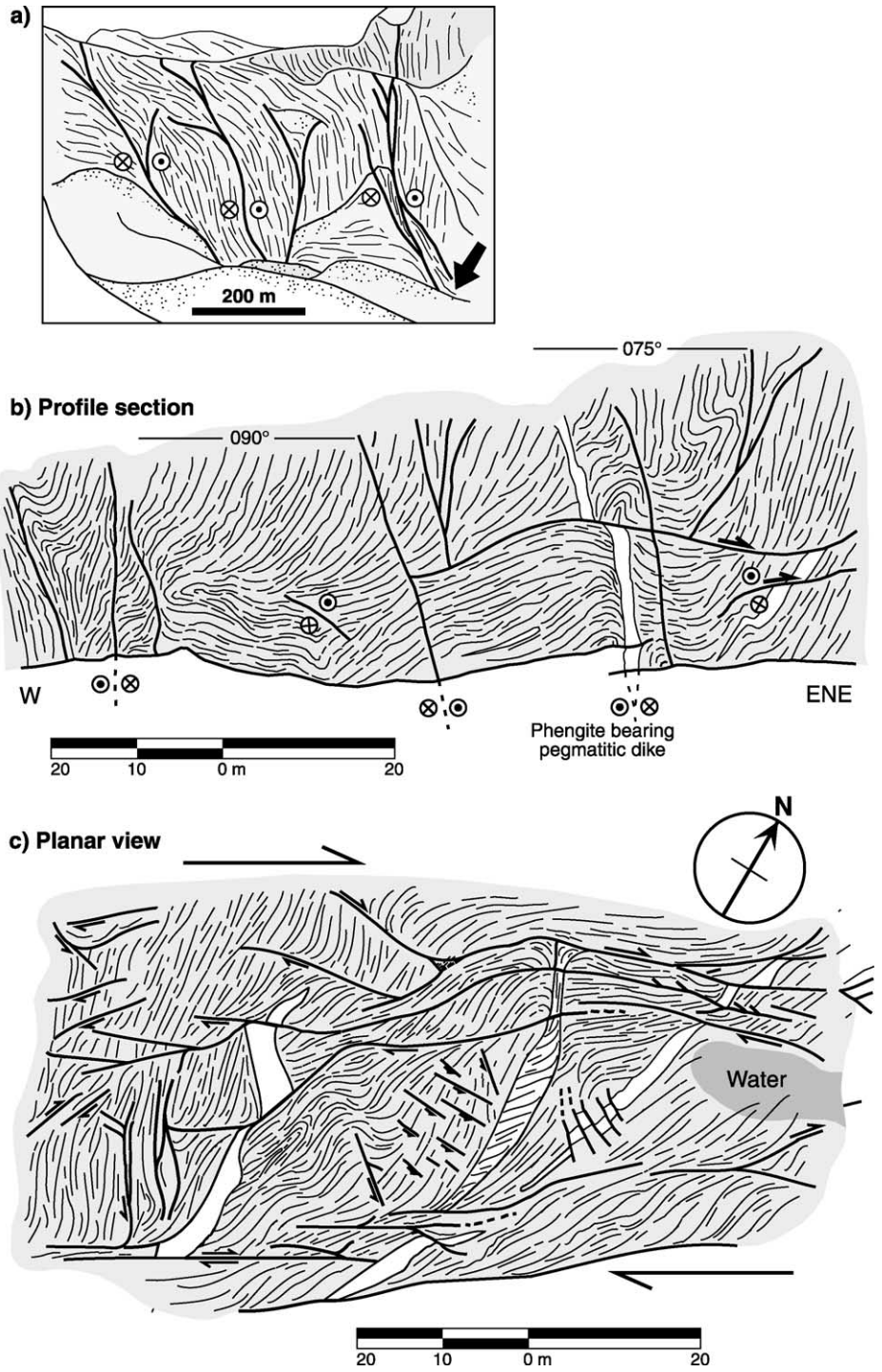
a)
200 m
075°
b) Profile section
090°
W
ENE
Phengite bearing
pegmatitic dike
20 10 0 m 20
N
c) Planar view
Water
20 10 0 m 20

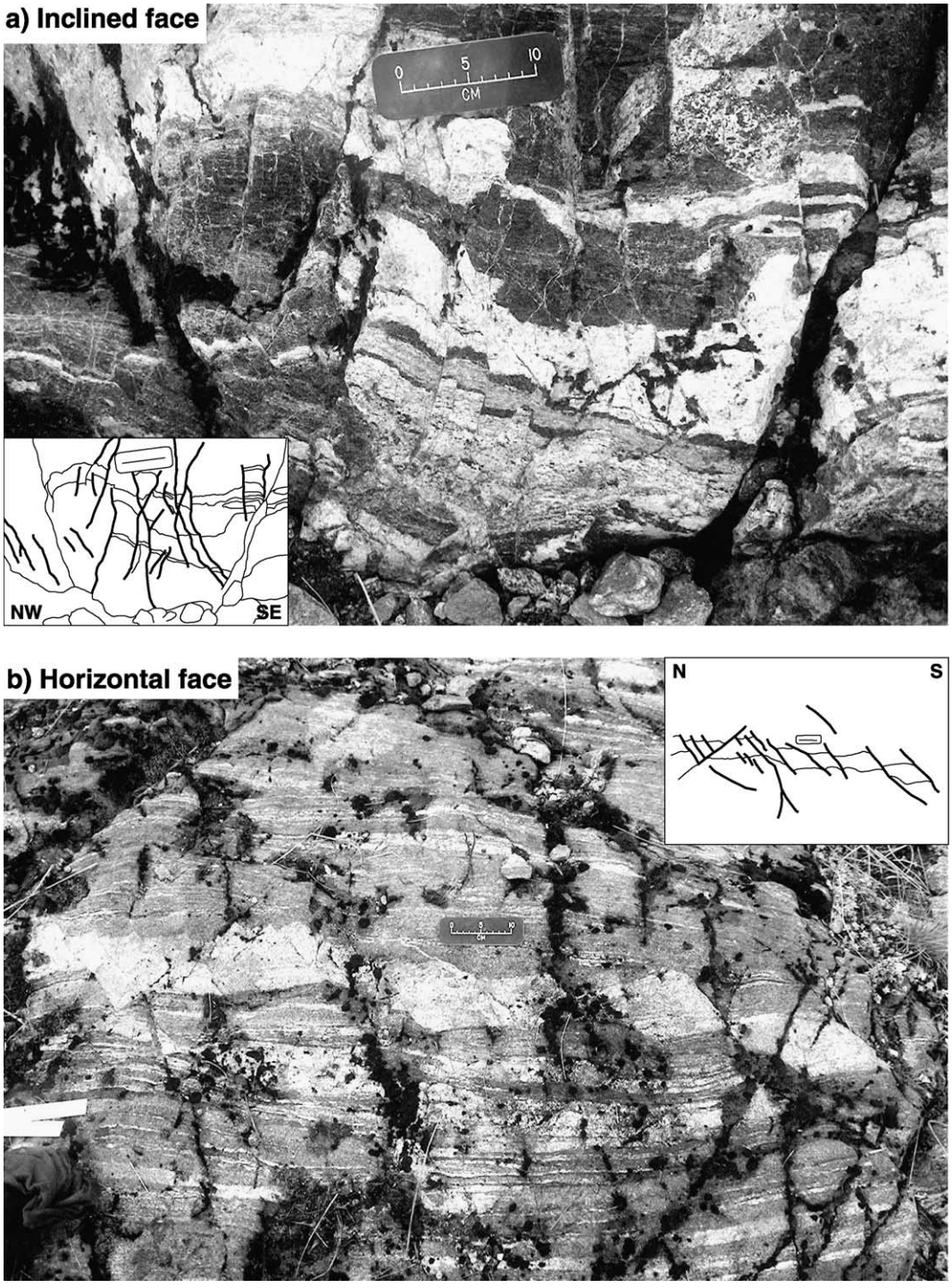

Fig. 5. (a–b) Photographs and sketch interpretations showing faulted dioritic dikes of the Harrison Gneiss (dikes parallel S_1 foliation) from Lake Never Never (see Fig. 3a for location). (a) Inclined face dipping approximately 25° south, northwest is to the left. (b) Horizontal face with view to the east. Photos are of areas located several meters apart. Note Faults form two mutually crosscutting populations that dip steeply to the NW (left) and SE (right). Faults are secondary to the main traces of the Harrison–Kaipo fault zone.

~ 3 km long (Fig. 3a). These faults are dextral, strike to the NE and dip steeply to the SE and NW (avg. strike 049°; avg. dip 80° to the SE). In most places, including at the contact between the Harrison and Milford gneisses, these faults parallel S_1. In others places, such as at the eastern boundary of the Harrison Gneiss, they cut and locally reorient S_1. The faults in this first dextral set form a stepwise, en echelon geometry that displace the eastern contact of the Harrison Gneiss by 7–8 km (Fig. 3a). This estimate reflects NE-striking fault planes and NE-plunging slip vectors. Epidote and quartz mineral striae occur ubiquitously on fault planes. These striae are mostly gently plunging to the NE and SW but also display some steep plunges. These data indicate that the dominant faults at the southeastern boundary of the Arthur River Complex strike parallel to the Alpine Fault (055°) and at trends of 049°, and accommodated mostly dextral strike-slip displacements with a subordinate component of oblique-dextral slip.

The second population contains sinistral faults that are subordinate to the first in terms of trace length and magnitude of displacement. Maximum trace lengths are ~ 2 km. Offsets along these faults are consistently sinistral and typically less than 100 m. These faults are subvertical and strike to the NNW and WNW (avg. strike 349°; avg. dip 88° to the SW). Epidote and quartz mineral striae show gentle to moderate plunges.

On horizontal surfaces, the two fault populations form stepovers and curvatures that outline asymmetric wedges of orthogneiss (Fig. 4c). This geometry is nearly identical to the strike-slip duplexes described by Woodcock and Fischer (1986). Discordant S_1 traces inside these wedges indicate that a component of strain within the fault zone was accommodated by block rotation between subparallel faults at the local scale. In profile, the two fault sets form branching palm tree-type geometries (Figs. 3f and 4a,b) that are detached by a series of subhorizontal décollements (Fig. 4b). Individual basal detachment faults exhibit trace lengths of up to several hundred meters along the walls of canyons and valleys. Small wavelength folds of S_1 formed adjacent to many of these branching faults and display highly variable geometries.

A characteristic feature of the Harrison–Kaipo and Pembroke fault zones is the occurrence of upper greenschist facies ductile shear zones (L_2–S_2) that cut the steep S_1 foliation of the Harrison Gneiss but also are cut by many of the brittle faults described above (Fig. 6a). These shear zones contain mylonitic foliations (S_2) and gently plunging mineral lineations (L_2) defined by aligned chlorite, phengitic white mica, and quartz aggregates. The L_2–S_2 fabric envelops augen-shaped lenses of retrogressed Harrison and Milford gneiss (Fig. 6a). S_1 within these lenses are truncated and dragged into parallelism with S_2. This pattern indicates that block rotation during ductile flow within these shear zones also was an important mechanism of accommodating displacements.

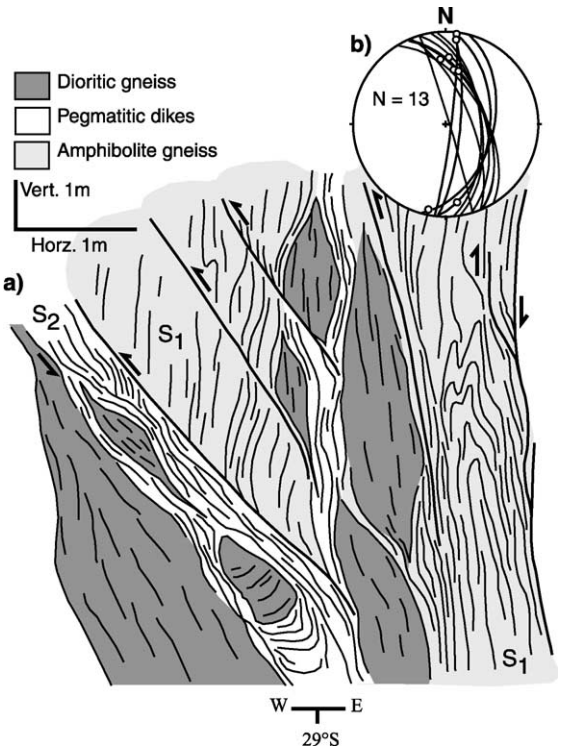

Fig. 6. (a) Oblique section (slab dips 29° to the south) showing the geometry of upper greenschist facies mylonitic shear zones in the Harrison–Kaipo fault zone at a site located 0.5 km north of Lake Never Never (see Fig. 3a for lake location). Shear zones envelop blocks of older amphibolites and dioritic gneiss of the Harrison Gneiss. The dominant foliation in the lenses (S_1) is cut by mylonitic S_2 foliations of the fault zone. Mylonitic S_2 foliations are overprinted and reactivated by brittle faults (thick black lines). (b) Lower hemisphere equal-area stereoplot of S_2 foliations. Lineations (circles) shown are axes of F_2 folds of S_1 which parallel biotite–chlorite mineral lineations.

All of the upper greenschist facies shear zones were intruded by swarms of coarse grained, white mica-, quartz-, and plagioclase-bearing pegmatitic dikes (Fig. 6a). Some dikes locally contain the L_2–S_2 fabric, others truncate it indicating that they were syntectonically emplaced during deformation. Sets of upright, tight to isoclinal folds (F_2) of dikes and of the L_1–S_1 fabric occur between steep mylonitic splays within these shear zones (Fig. 6a). Many of these F_2 folds display axial surfaces that parallel S_2 and the boundaries of the shear zones. Most fold axes plunge gently to the N and S parallel to L_2 (Fig. 6b). The margins of these dikes localized brittle faults and display cataclastic textures and fault gouge (Fig. 6a).

At the western boundary of the Arthur River Complex, the Pembroke fault includes numerous splays that strike to the NE and are subvertical to steeply dipping to the west. Subvertical splays of the Pembroke fault merge with the northernmost seg-

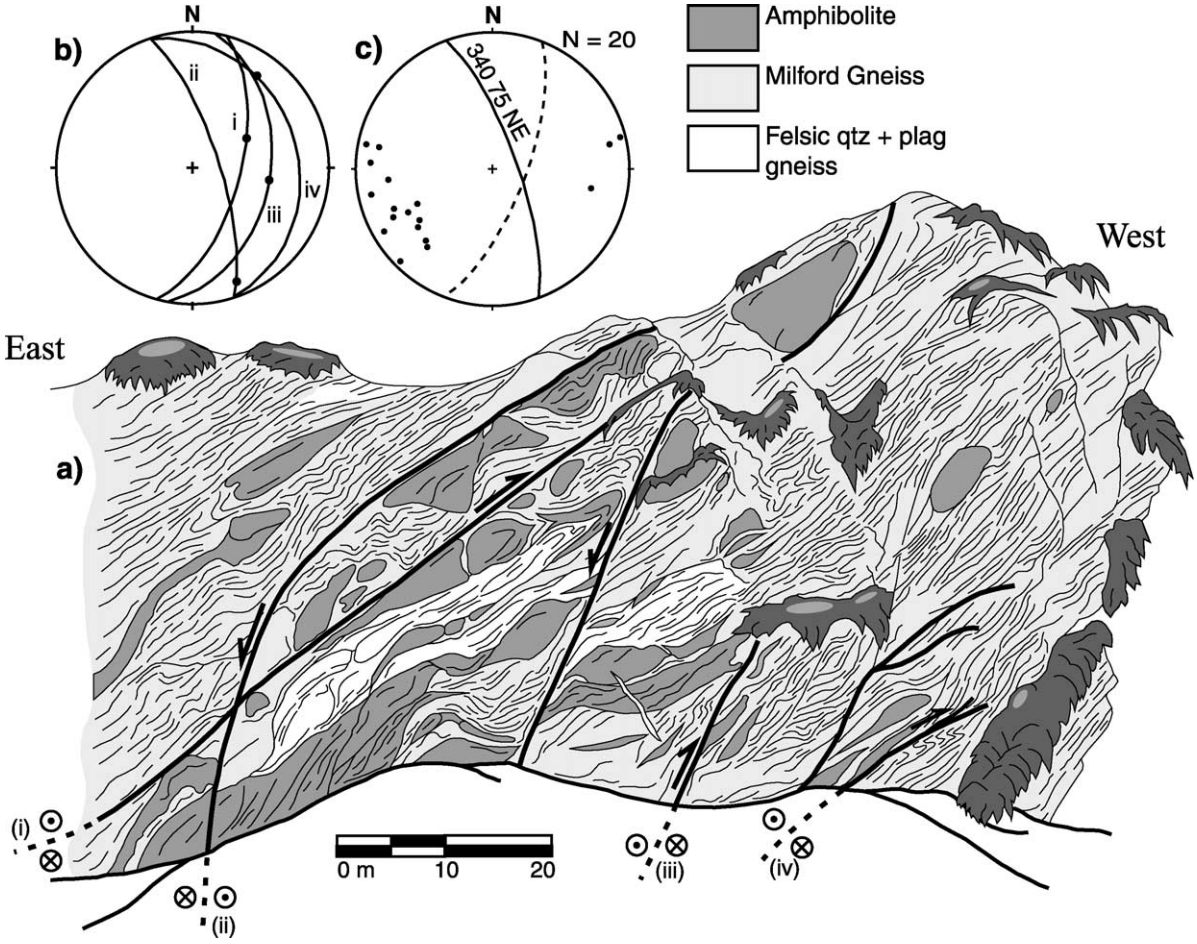

Fig. 7. (a) Vertical section of cliff face (looking south) near Mt. Ongaruanuku (site MO in Fig. 3a). Faults are curved oblique-dextral-reverse faults that show a component of either normal or reverse vertical offset (indicated by half arrows) indicative of a vertical shuffling of fault blocks. See text for discussion of sense of shear indicators. Foliation shown is a recrystallized (upper greenschist facies) S_1 foliation in the Milford Gneiss. (b) Lower hemisphere equal-area stereoplot showing orientation of the four faults (i, ii, iii, and iv) and corresponding slickenlines (dots) shown in (a). (c) Lower hemisphere equal-area stereoplot showing average orientation of S_1 in footwall of oblique-reverse faults (solid great circle) and average for all of domain 2 (dashed great circle).

ments of the Harrison–Kaipo fault. Blattner (1991) reported fault strikes between 20° and 45° and dips of approximately 70° to the west for the main trace of the Pembroke fault. We observed steep splays of this fault along the margins of the Anita ultramafites and Milford Gneiss at Poison Bay (Fig. 2) that also strike to the NE and dip ~ 65° to the west. Fault surfaces preserve gently plunging (~ 5°) talc and epidote striae on fault surfaces.

4.2. Domain 2: reverse and oblique-slip faults and related structures

In domain 2, the largest fault traces in the Harrison–Kaipo fault zone curve to strike to the N and NNE before it abuts against the NE-striking Pembroke fault (Fig. 3). Most faults in domain 2 dip gently to moderately to the E, SE, and SW (avg. strike 359°; avg. dip 52° to the SE; Fig. 7). Mineral striae and slickenlines also are different than those in domain 1. Slip on these faults deformed S_1 in the Milford Gneiss into asymmetric lenses in profile, similar to the shapes of the fault-bounded lenses on horizontal surfaces at Lake Never Never (Fig. 4). Tight, inclined folds of S_1 between curved fault segments reflect contraction between brittle faults (Figs. 3f and 6).

One important geometric characteristic of domain 2 is the opposing dip of some oblique-slip fault segments near and south of Mount Ongaruanuku (Fig. 3f). These faults divide the Milford Gneiss into a series of fault-bounded wedges, across which there is significant vertical offset. For up to 2 km east and west of the faults mapped at Mount Ongaruanuku both normal and reverse separations (viewed in profile) occur across these faults (Fig. 7). This style of normal and reverse offset across steep faults is characteristic of positive flower structures (following definition of Harding, 1985) and is described by Sylvester (1988) as vertical porpoising (or shuffling) of fault blocks during convergent strike-slip faulting. We observed this phenomenon at the cm-scale (see also photo Fig. 4c of Clarke et al., 2000) and at the km-scale. These data indicate that crustal fragments of the Arthur River Complex were extruded vertically and shuffled between faults of opposing dip between the Pembroke and Harrison–Kaipo fault zones.

5. Kinematic analysis

5.1. Microstructures and sense of shear indicators

In the ductile parts of the Harrison–Kaipo and Pembroke fault zones mylonitic foliations are defined by the upper greenschist facies assemblage biotite, chlorite, quartz, plagioclase, and phengitic white mica. These mylonites contain large (8–25 mm) plagioclase augen that are inherited parts of Early Cretaceous assemblages. The augen display undulose extinction, microkinks and microfractures. Brittle failure was the dominant deformation mechanism in feldspars surrounded by a quartz–mica matrix (Fig. 8). However, in some grains, fine-grained, recrystallized plagioclase occurs along serrated grain boundaries. These subgrains shows an increase in albite content relative to the compositions of the larger and older Early Cretaceous plagioclase grains. These features and the presence of tapered deformation bands indicate that microfracturing of plagioclase was assisted by dislocation glide. The occurrence of dislocation glide suggests temperatures of deformation ≥ 400°C (Passchier and Trouw, 1996).

Quartz grains display undulose extinction, patchy subgrains, core–mantle structures, and diffuse, serrated grain boundaries indicative of grain size reduction via rotational recrystallization and grain boundary migration (Fig. 8). Polygonized quartz ribbons wrap large plagioclase grains. Kinked biotite and phengitic white mica define cleavage planes that parallel the quartz ribbons. The occurrence of grain boundary migration and recovery processes in quartz also suggest $T \geq 400$°C (Passchier and Trouw, 1996).

We identified the following microstructures in the mylonites, all of which are suitable as sense of shear indicators: preferred lattice orientations in quartz, asymmetric mica fish, asymmetric mantled porphyroblasts, oblique foliations, and shear band cleavages (S–C and C′ types). All structures were viewed on surfaces oriented perpendicular to foliation and parallel to mineral lineations. Boudinaged dikes in outcrop and stretched plagioclase grains in thin section indicate that the mineral lineation represents a true stretching direction. C-planes in S–C fabrics and C′ shear band cleavage planes were defined by white mica, chlorite and biotite.

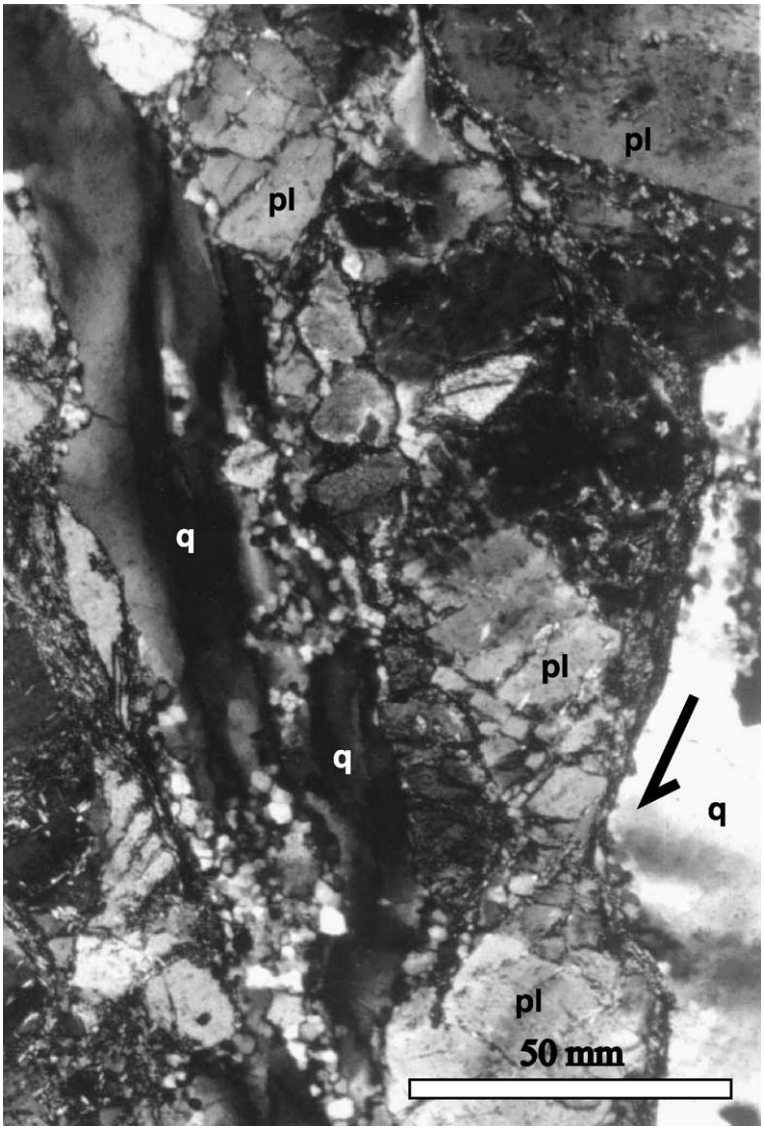

Fig. 8. Photomicrographs (crossed polars) of deformed upper greenschist facies assemblage in the Harrison–Kaipo fault zone. Note dynamically recrystallized quartz (q) ribbons and faulted (arrow) plagioclase (pl) grain. Plagioclase shows evidence of cataclasis along grain boundaries. Scale bar is 50 μm. See text for discussion.

Brittlely deformed segments of the fault zones contain cataclastically deformed plagioclase, hornblende and quartz. Epidote mineralization occurred on most fault surfaces. For sense of shear indicators in these fault segments, we used conjugate microfaults in thin section and macroscopic sense of shear indicators including offset veins and dikes (Fig. 5), asymmetric lozenges of gneiss bounded by faults (Fig. 4c), and duplex-style thrust horses in zones of reverse and oblique-reverse shear (Fig. 7). Microfaults oriented parallel or at low angles to the foliation plane showed dextral offsets. Microfaults that exhibit sinistral offsets are oriented at high angles to the foliation. The sinistral offsets and high angle of these microfaults suggests that this set is antithetic to a dominantly dextral sense of shear. All structures indicated a scale-

invariant oblique-dextral sense of shear for the main NE-striking traces of the Harrison–Kaipo fault zone and oblique-dextral reverse displacements on the N-striking segments.

Asymmetric tails on plagioclase augen indicated a dominantly dextral sense of rotation within the shear zones. The tails are composed of quartz–feldspar aggregates and elongate lathes of chlorite, biotite and

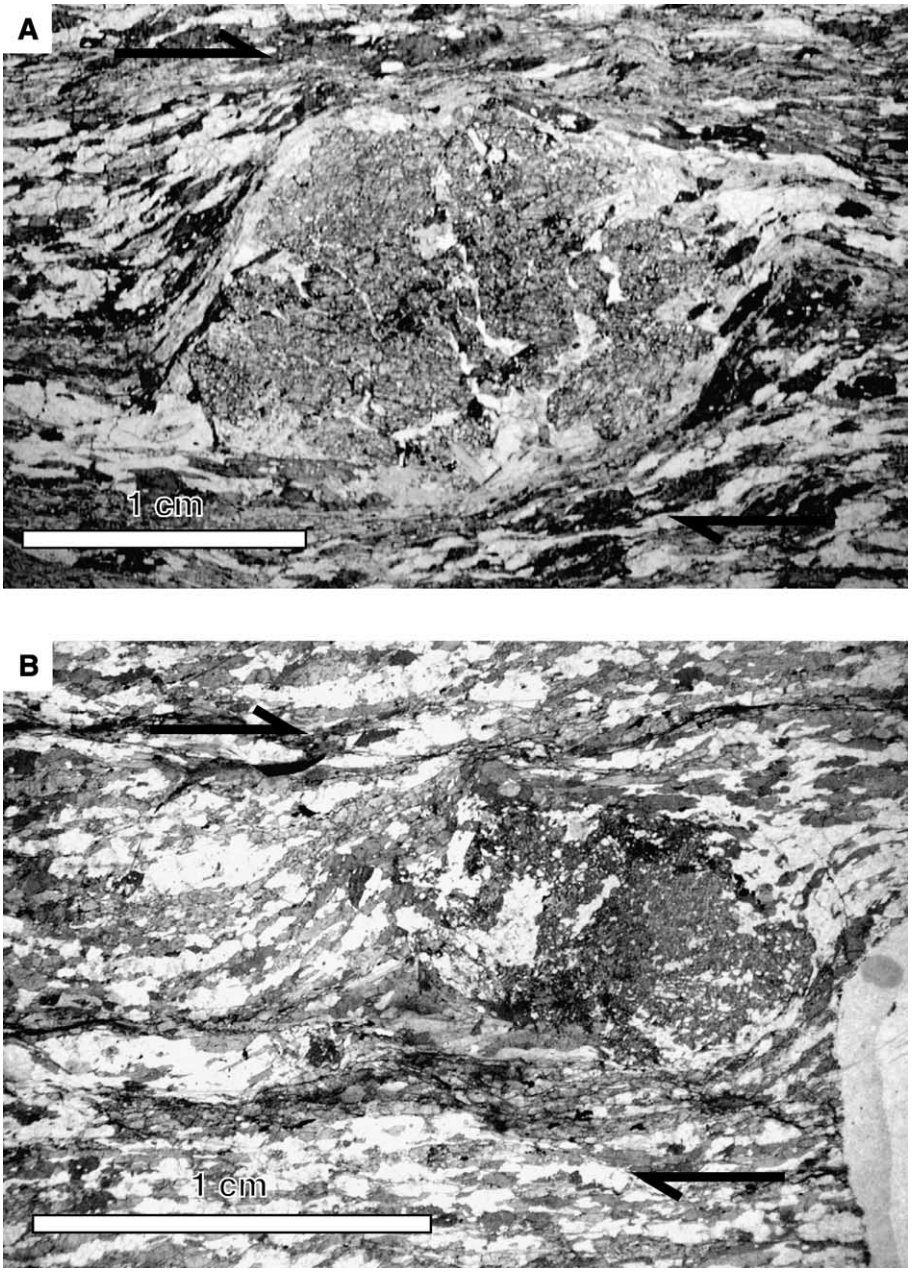

Fig. 9. (A) Asymmetric tails composed of chlorite, quartz and biotite on forward (clockwise) garnet forming a σ-type geometry. Sense of shear is dextral. Scale bar is 1 cm. (B) Asymmetric tails composed of chlorite, quartz and biotite on backrotated (counterclockwise) garnet forming a β-type geometry. Sense of shear is also dextral. Scale bar is 7 mm.

white mica and show mostly σ-type stair-stepped geometries (Fig. 9A) with a few δ-type clasts. However, an important subset of these grains rotated backwards with respect to the dominant dextral shear sense (Fig. 9B). Back rotation (following Simpson and De Paor, 1993) is indicated by elliptical grains with long axes oriented at high angles to the foliation that are tilted in the opposite direction to the σ-type grains. In addition, the tails of chlorite and biotite grew on the broad sides of these grains, not on the tips as in the σ-type grains (Fig. 9B). These β-type tails indicate that a component of horizontal pure shear characterized displacement within the Harrison–Kaipo and Pembroke faults. This is consistent with interpretations of transpressional deformation east of the Alpine Fault (Norris et al., 1990).

5.2. Fault-slip data

In this section, we present average fault plane solutions for the three fault populations that compose the Harrison–Kaipo and Pembroke fault zones (Fig. 10). We used a three-dimensional, instantaneous strain analysis of fault-slip data to determine the bulk kinematics of different fault segments and the orientations of the principal axes of incremental strain. This technique employs the moment tensor summation commonly used in earthquake studies which characterizes the infinitesimal strain due to fault rupture during an earthquake. Previous work indicates that strains due to faulting must exceed ~60% before use of instantaneous strain axes produce errors greater than typical field data (Cladouhos and Allmendinger, 1993). In our case, this approach is valid because displacements along the faults used (most with orders of magnitude ranging from centimeters to one hundred meters, some ranging up to several kilometers) are small compared to the total strain resulting from oblique plate convergence. Total strains involved ~ 70 km of shortening normal to the Alpine Fault and 460 km of fault-parallel displacement on the Alpine Fault (Walcott, 1998; Norris and Cooper, 2001).

We calculated the principal axes of shortening (Z) and extension (X) for the incremental strain tensor associated with each fault using measurements of fault plane attitude, slip-vector pitch (striae orientation), and sense of displacement for each fault. Sense of displacement was deduced using measured offsets of veins, dikes, lithologic bands and other markers within the Harrison and Milford gneisses. We focused our analysis in five areas of near 100% exposure to ensure that faults of all possible orientation were measured allowing us to justify the assumption that the faults are representative of the main populations. Underestimation of the total number of faults is only important in calculation of the total amount of strain (Cladouhos and Allmendinger, 1993). Important sites included areas surrounding Selwyn Creek, Lake Pukutahi, the Harrison Valley, Lake Never Never, and Mount Ongaruanuku. We also assumed an identical age of deformation along all faults, which appears reasonable on the basis of crosscutting relationships and available isotopic ages (discussed in the next section).

The strain axes X and Z for each fault plane lie at 45° to both the fault normal and slip vector (slickenline orientation). Sense of slip allows distinction between the X and Z axes, the intermediate axis (Y) lies perpendicular to both X and Z. No interpretation is

Fig. 10. Fault-slip data and kinematic solutions for fault populations discussed in the text. (a) to (h) are representative of domain 1 faults and (i) to (l) are representative of domain 2 faults. All plots are lower hemisphere equal area stereoplots. (a), (e) and (i) (left most column) show plots of three fault populations distinguished on the basis of orientation, trace length and sense of displacement. Fault planes are great circles, slickenlines are black dots; arrow shows direction of motion of hanging wall for each fault population. Number (N) of faults measured for each set shown. (b), (c), (f), (g), (j) and (k) (middle two columns) show contoured plots of contractional axes (Z, black dots) and extension axes (X, open squares) for each of the three fault populations. Contouring by the Kamb (1959) method shows contours at 2.0, 4.0, 6.0, 8.0, and 10.0 sigma. (d), (h), and (l) (right-most column) show average kinematic solutions calculated for each fault population using the methods of Marrett and Allmendinger (1990). Plots generated using Faultkin v3.8 computer program written by R.W. Allmendinger, R.A. Marrett, and T. Cladouhos. This program constrains the X, Y and Z directions of the incremental strain ellipsoid to be oriented 90° from one another. Axes of shortening (Z, solid circles) and extension (X, open squares) for the incremental strain tensors for each fault measured are shown superimposed on the average kinematic solution. Bold solid squares represent directional maxima of shortening (Z) and extensional (X) axes for average incremental strain solution for fault set. Intermediate axis (Y) also shown. Bold lines are modelled faults, half arrows show sense of slip on fault. See text for discussion of methods and interpretation.

involved in this determination, the result is simply a manipulation of the fault-slip data. An average kinematic solution for each fault population is then calculated using linked Bingham distribution statistics to determine the directional maxima of the X and Z strain axes for the fault arrays (Marrett and Allmendinger, 1990). This method of is equivalent to the numerical summation of Molnar's (1983) asymmetric moment

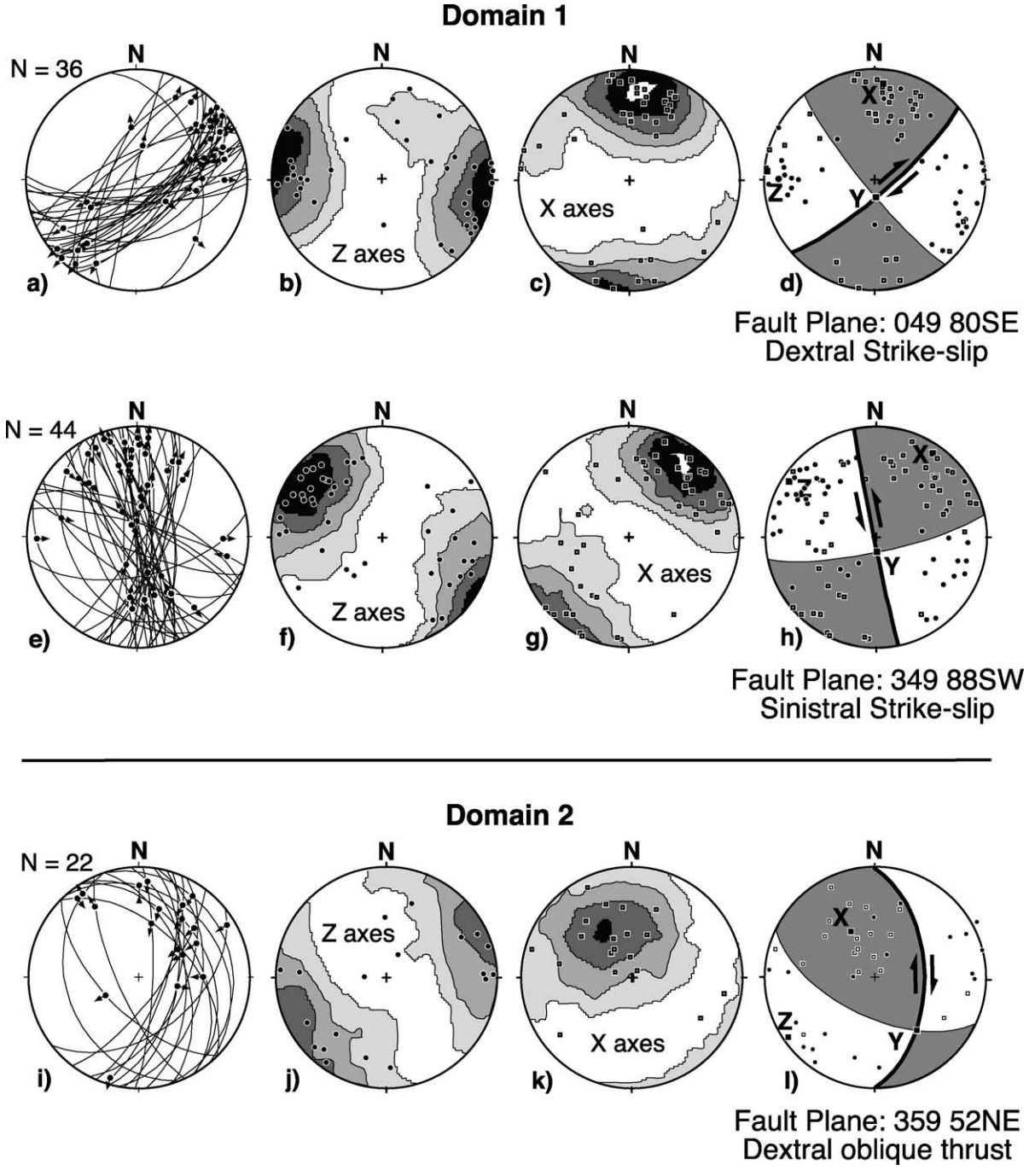

tensor where individual faults are weighted equally and assumes the faults are scale invariant (Marrett and Allmendinger, 1990).

The average fault plane solutions show graphically the bulk kinematics for each population of faults measured (Fig. 10a,e and i). Average orientations of the incremental strain axes are shown in separate plots contoured using the Kamb (1959) method (Fig. 10b,c,f,g,j and k). These plots show that the strain axes for three fault populations form coherent clusters despite kinematic heterogeneity. A positive test of our results is that the strain axis maxima in the contoured plots and the average *X* and *Z* directions calculated using linked Bingham statistics show good agreement. The modelled fault orientations, shown as bold lines (Fig. 10d,h and l), parallel the average orientations of the three populations measured.

Dextral faults from domain 1 show mostly strike-slip displacements on a fault plane that on average strikes 049° and dips steeply 80°SE (Fig. 10d). Sinistral faults from domain 1 also show mostly strike-slip displacements on a fault plane that on average strikes 349° and dips steeply 88°SW (Fig. 10h). Faults from domain 2 show oblique-dextral and reverse displacements on a fault plane that on average strikes 359° and dips moderately 52°NE (Fig. 10l). The modelled fault orientations, shown as bold lines (Fig. 10d,h and l), parallel the average orientations of the three populations measured. A kinematic solution incorporating all faults measured in domain 1 shows that the main fault traces of the Harrison–Kaipo and Pembroke fault zones accommodated bulk dextral displacements on steep NE-striking segments with a small oblique component (Fig. 11).

6. Ages of deformation and metamorphism

We obtained eight $^{40}K-^{39}Ar$ mineral ages on phengitic white mica from upper greenschist facies shear zones in the Saint Anne Gneiss at Poison Bay (Table 1; Fig. 2). These fabrics formed in splays of the Alpine and Pembroke faults at the western boundary of the Anita Shear Zone. Analytical procedures are discussed in Appendix A.

We analyzed two size fractions from four samples collected from the greenschist facies shear zones (Table 1). Two clusters of ages at 12–13 and 20–30 Ma are evident in both size fractions, suggesting that two periods of mineral growth or recrystallization accompanied deformation within these shear zones. The 20–30 Ma cluster may indicate that slip along the Alpine Fault and oblique-reverse slip east of the fault began during this interval. This interpretation is consistent with K–Ar ages of ~ 25 Ma obtained by

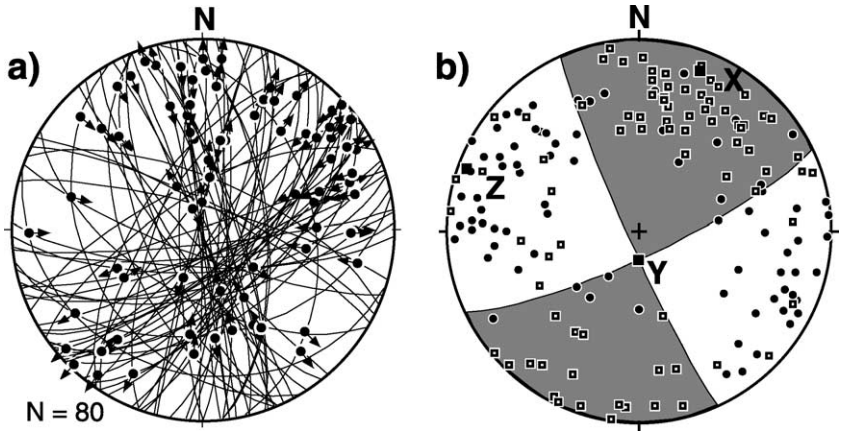

Fig. 11. Bulk kinematic fault plane solution for the main dextral traces of the Harrison–Kaipo fault zone. Solution incorporates all oblique-dextral and oblique sinistral fault populations (Fig. 10a and e). (a) Lower hemisphere equal area stereoplot of slip vectors from domain 1. Note kinematic heterogeneity involving complex horizontal and vertical displacements. Fault planes deleted for clarity. (b) Kinematic fault plane solution. Modelled fault plane strikes 065° and dips 79° to the SE. Nodal plane strikes 336° and dips 85° to the SW. See text for discussion.

Table 1
K–Ar ages obtained from mylonitic splays of the Pembroke and Alpine Fault zones

Sample	Size fraction [μm]	K [%]	$^{40}Ar^{a}$ [mol/g]	$^{40}Ar^{a}$ [%]	Age $\pm 2\sigma^{\S}$ [Ma]
97100G	(+180)	5.79	1.2606e−10	65.34	12.50 ± 0.21
97100E	(+180)	6.50	1.4279e−10	79.36	12.63 ± 0.22
97113B	(+180)	4.17	2.1665e−10	85.73	29.73 ± 0.49
97114	(+180)	3.64	1.3615e−10	84.88	21.45 ± 0.56
97100G	(+106)	6.10	1.3394e−10	64.71	12.62 ± 0.22
97100E	(+106)	6.29	1.4527e−10	77.45	13.27 ± 0.24
97113B	(+106)	6.37	2.2982e−10	84.76	20.68 ± 0.37
97114	(+106)	7.41	1.7089e−10	85.00	13.25 ± 0.31

The error for Argon analyses was below 1.50% and the $^{40}Ar/^{36}Ar$ value for airshots averaged 294.39 ± 0.201 (2σ, $n=5$). The K–Ar ages were calculated using ^{40}K abundance and decay constants recommended by Steiger and Jäger (1977). The age uncertainties shown are within 2σ and include errors acquired during sample weighing, $^{38}Ar/^{36}Ar$ and $^{40}Ar/^{38}Ar$ measurements and K analysis. See Appendix A for description of analytical procedures.

[a] Radiogenic argon.

[§] $\lambda_{\beta}=4.963\times10^{-10}$ year^{-1}; $\lambda_{\varepsilon}=0.581\times10^{-10}$; $^{40}K/K=1.167\times10^{-4}$.

Cooper et al. (1987) from lamprophyre dikes within the Alpine Fault north of Fiordland and ^{40}Ar–^{39}Ar evidence for rapid cooling at the eastern edge of the Darran Complex beginning at ~ 20 Ma (Mortimer et al., 1999). They also are consistent with evidence of early Miocene basin inversion east of the granulite belt, which likely involved some strike-slip activity (Norris and Turnbull, 1993). Alternatively, the 20–30 Ma scatter could represent a mix of Tertiary and Cretaceous cooling ages (Geary and Paterson, 1990).

The younger 12–13 Ma interval we determined is slightly older than the 7–9 Ma ages reported by Nathan et al. (2000) from muscovite and biotite in the Saint Anne Gneiss at Milford Sound. Both our data and those of Nathan et al. (2000) indicate that dextral shear involving growth or recrystallization of phengitic white mica occurred during the middle–late Miocene. This interpretation is consistent with the age of similar styles of reverse and oblique-dextral faulting east of the Fiordland granulites which initiated in the early Miocene (Norris and Turnbull, 1993). On the basis of similar structural styles, kinematics, metamorphic grade, and the occurrence of syntectonic white mica-bearing pegmatites we correlate the upper greenschist facies shear zones at the northwestern and southeastern boundaries of the Arthur River Complex. If this correlation is correct, then the crosscutting relationships among these greenschist fabrics and all brittle faults used in this study suggests that the faults recorded slip that is younger than 7–9 Ma, the youngest ages reported by Nathan et al. (2000). We discuss additional supporting evidence for this interpretation in the discussion section below.

7. Discussion: deformation processes and tectonic implications

Our results allow us to address the following issues: (1) The partitioning of horizontal and vertical displacements east of the Alpine Fault; (2) the effects of Late Tertiary deformation on the evolution and exhumation of Fiordland's high-*P* granulite belt; and (3) how the segment of the Alpine Fault and adjacent areas we examined compare with sections located farther north and south.

7.1. The partitioning of vertical and horizontal displacements within and adjacent to Fiordland

Since 6.4 Ma, a total of ~ 70 km of shortening between the Australian and Pacific plates has been accommodated across the southernmost onshore segment of the Alpine Fault (Walcott, 1998). Observations in the Otago region suggest that only ~ 10 km of shortening occurs in the 150–200 km zone east of Fiordland (Norris et al., 1978) and that most of the required 70 km likely occurs adjacent to the eastern boundary of the Fiordland Block (Norris and Turnbull, 1993). This eastern boundary coincides with the Moonlight and Fiordland Boundary faults. These faults are seismically active (Anderson et al., 1993) and are thought to have accommodated some 20 km of dextral strike-slip motion and ~ 30 km of north–south shortening since the late middle Miocene (Norris and Turnbull, 1993). Our data allow for 6.5–7.0 km of additional oblique-dextral and reverse displacements northwest of the Moonlight fault system in northern Fiordland. This result also is consistent with a focusing of contractional deformation in the mountainous terrain along Fiordland's northeastern boundary.

In addition to reverse and strike – slip faulting, horizontal displacements east of the Alpine Fault likely are accommodated along flat-lying detachments faults. Koons and Henderson (1995) postulated that upper crustal shortening in western Otago is accommodated at depth by a low angle detachment fault. Profiles across the central regions of the fault zone indicate that a moderately dipping Alpine Fault shallows downward into one of these horizontal detachments located at the base of the crust (e.g., Norris et al., 1990; Sutherland et al., 2000). Our data indicate that a similar style of horizontal faulting may also play a role in accommodating deformation beneath Fiordland. We noted that the style of deformation observed at the outcrop scale within Fiordland strongly resembles the style of deformation observed at the scale of tens of kilometers. For example, the palm tree structures observed in creek sections also occur at the scale of all of northern Fiordland (compare (Figs. 3f, 4b and 12)). This suggests that the subhorizontal detachment faults we observed in the Harrison–Kaipo and Pembroke fault zones reflect similar structures that occur at the scale of all of northern Fiordland.

Significant vertical displacements are intrinsic to all transpressional regimes (Fossen and Tikoff, 1998). The manner in which these displacements are partitioned is important for understanding the exhumation of Fiordland's high-*P* granulite belt. Earthquake studies (Anderson et al., 1993; Doser et al., 1999; Moore et al., 2000) suggest that a combination of oblique-slip and reverse displacements along the boundaries of Fiordland crust combined with erosion (Koons, 1994) resulted in the vertical uplift and exhumation of some of Fiordland crust. Norris and Turnbull (1993) describe a restraining bend model that explains how reverse and strike-slip displacements were linked during this process. Localized vertical displacements on steep faults also were postulated by Rattenbury (1986, 1991) to explain the exhumation of the high grade Fraser Complex located north of Fiordland. But can this mechanism explain the exhumation of the Fiordland granulite belt relative to adjacent rocks, and if so by how much?

Thermochronologic data indicate that the northern Fiordland granulite belt had cooled to 300–400 °C by ~ 90 Ma (Mattinson et al., 1986; Nathan et al., 2000), implying that a maximum of ~ 10 km of exhumation occurred since that time. Sutherland (1996) used displaced Miocene–Pliocene conglomerate units to suggest that 1–6 km of exhumation has affected the high-*P* granulites since ~ 5 Ma. Our results indicate that this exhumation most likely occurred as fault-bounded wedges were shuffled vertically and squeezed up between curved reverse and oblique-slip faults at the northern edge of the Fiordland belt. The Arthur River Complex and the Darran Complex constitute two of these wedges that have been displaced relative to one another (Fig. 12). Blattner (1991) and Tulloch et al. (2000) observed significant vertical offsets across the Glade–Darran fault and the Surprise Creek fault, respectively, that suggest this process affected all of northern Fiordland. One effect of these vertical displacements was the exhumation of the ductile roots of the Harrison–Kaipo and Pembroke fault zones we observed along the boundaries of the Arthur River Complex.

Our structural and metamorphic data also provide two ways of evaluating the amount and timing of vertical displacements and exhumation. First, 6.5–7.0 km of displacement have accumulated within en echelon traces of the Harrison–Kaipo fault zone. These en echelon traces are physically linked to moderately E- and NE-dipping (30–52°) reverse faults (Fig. 3) indicating that the 6.5–7 km of displacement also must have been accommodated by the reverse faults. This linkage and the range of dip angles and slip vectors displayed by the faults we measured allow 3.0–5.5 km of vertical displacement along dipping faults at the northern edge of the granulite belt assuming 7 km of total oblique-slip displacement. If our correlations of brittle faults and mylonitic fabrics across northern Fiordland are correct then this displacement occurred since 7–9 Ma.

Second, we obtained temperature estimates of ≥ 400 °C for deformation in the exhumed mylonitic parts of the fault zones. The youngest phase of upper greenschist facies deformation is 7–9 Ma. Fluid inclusion studies in the central part of the Alpine Fault suggest that high temperatures of 310–350 °C occur at 6–8 km below the transform (Holm et al., 1989). These values imply a shallow brittle–ductile transition at 5–6 km east of the Alpine Fault. These data, the temperature range of the exhumed mylonites in Fiordland, and the age of the brittle faults suggest a maximum of 6 km of exhumation could have occurred since 7–9 Ma. This maximum value of 6 km matches

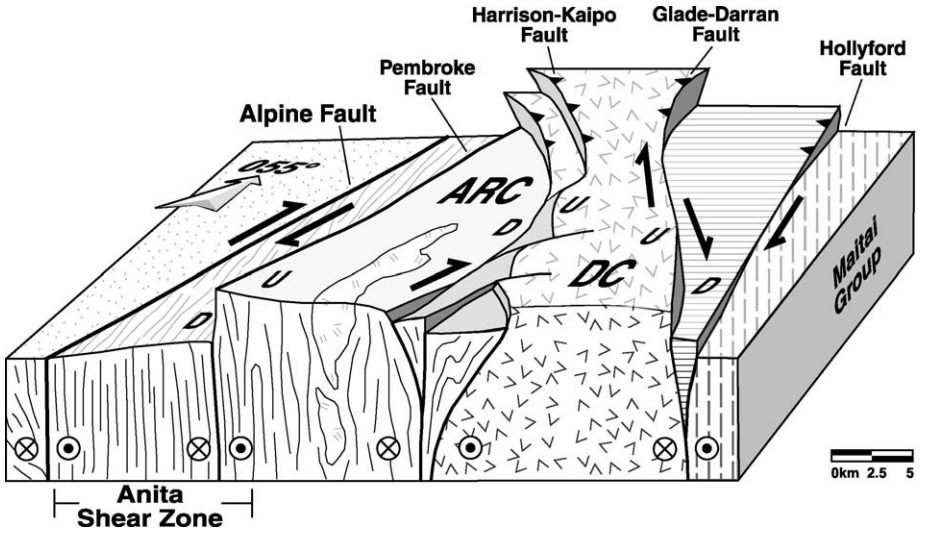

Fig. 12. Block diagram of region north of Milford Sound showing the wedge-shaped, palm tree style geometry created by steep, branching faults of the Pembroke and Harrison–Kaipo fault zones. Oblique-slip and reverse motion have resulted in the vertical displacement of the Arthur River Complex (ARC) and the Darran Complex (DC) relative to adjacent wedges. Patterns correspond to those in Fig. 2. Arrows show relative senses of horizontal displacements. Relative vertical displacements are shown as down (D) and up (U). No vertical exaggeration.

the upper limit of vertical displacement obtained by Sutherland (1996) using Miocene–Pliocene conglomerate units.

Our estimate of 3.0–5.5 km of vertical displacement on the reverse faults we measured is substantially less than the estimate of 10 km of Late Tertiary exhumation predicted by the thermochronologic data. This discrepancy can be accounted for in several ways. First, some of the missing 5–7 km of vertical displacement likely was accommodated along other faults, including the Glade–Darran Fault (Fig. 2). Second, some exhumation and vertical displacement may have occurred prior to 7–9 Ma. Finally, other mechanisms in addition to reverse and oblique-slip faulting may have increased the amount of exhumation of the granulites during the Late Tertiary. We suggest that a combination of these three scenarios is most likely. The importance of erosion during exhumation is clearly indicated by increased sedimentation rates at 12 and 5 Ma and large volumes of Pliocene–Quaternary sediment (5–0 Ma) derived from southeast of the Alpine Fault (Sutherland, 1996). In addition, a flexural bending of the subducted Australian plate beneath Fiordland (Furlong et al., 2001) also likely increased exhumation rates since the change in plate motions at ~6.4 Ma. The possible importance of this latter process is supported by a large positive Bouger gravity anomaly (>150 mgal) over Fiordland and the high (>1 km) average elevation of the Fiordland ranges (Furlong et al., 2001).

7.2. Earthquake focal mechanisms

Published focal mechanisms (Anderson et al., 1993; Doser et al., 1999; Moore et al., 2000) for shallow (<24 km) earthquakes in the Fiordland region display oblique-slip solutions with reverse components that are similar to the kinematic solutions we obtained (Fig. 13). In all the solutions shown in Fig. 13, fault planes were chosen to coincide with the nodal plane that yielded dextral slip and that approximately paralleled either the Alpine Fault or the dextral faults we observed east of the Alpine Fault. In one case (event JB; Fig. 13) our selection of the fault plane deviated from the selection made in the original study (Doser et al., 1999). We chose the E-striking fault plane in this case because it yielded a trend and dextral kinematics that are similar to the dextral faults we measured in domain 1 (Fig. 10a). Slip vectors for each mechanism were calculated by assuming slip was accommodated along the nodal plane oriented

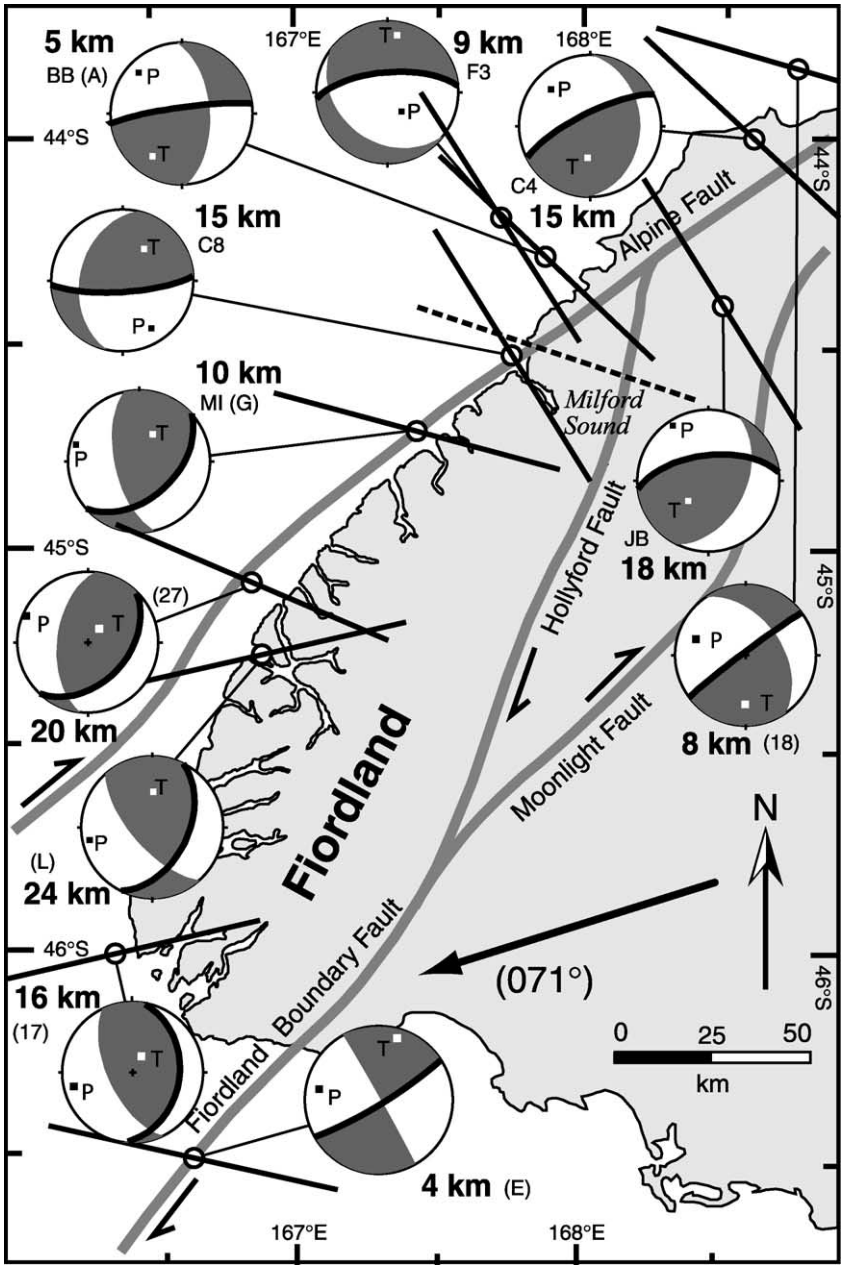

Fig. 13. Map of SW New Zealand showing shallow (<24 km depth) earthquake focal mechanisms from Anderson et al. (1993), Doser et al. (1999) and Moore et al. (2000). Circles show epicenters; dark black lines show orientations of maximum principal compression (*P*). Dashed line shows direction of minimum instantaneous shortening (*Z*) derived for northern Fiordland in this study. Depth of earthquakes also shown in km. Plate slip vector is from DeMets et al. (1994).

closer to parallelism with the plate boundary (Anderson et al., 1993; Doser et al., 1999; Moore et al., 2000). The orientations of the axes of compression (*P*) and tension (*T*) shown in Fig. 13 were calculated using the assigned fault planes and slip vectors.

An event located less than 20 km west of the Alpine Fault (BB; Fig. 13) shows nodal planes that lie oblique to the trend of the Alpine Fault (Doser et al., 1999). This solution, and another dextral solution located on the Fiordland Boundary Fault (E; Fig. 13), are most similar to the average fault plane solution we obtained for the Harrison–Kaipo fault zone (Fig. 11b). A 1976 event (MI, Fig. 13) that occurred 10 km below the mouth of Sutherland Sound shows oblique-dextral-reverse slip parallel to an E-plunging slip vector on a NE-striking fault plane (Anderson et al., 1993; Doser et al., 1999). The compressional (*P*) axis of this event is most similar to the average instantaneous shortening direction (*Z*) we calculated (Fig. 13). Three other earthquakes that occurred north (C4, C8, 18; Fig. 13) and one that occurred northeast (JB; Fig. 13) of Milford Sound yielded oblique-dextral slip with a reverse component on moderately NE- or ENE-striking fault planes (Doser et al., 1999; Moore et al., 2000). The fault planes, slip vectors, and senses of displacement implied by these solutions are similar to those we obtained for the dextral fault set in our domain 1 (compare with Figs. 10d and 11b). An event near Doubtful Sound (L; Fig. 13) and another located south of Fiordland (17; Fig. 13) show dominantly reverse slip on E-dipping planes (Moore et al., 2000) that are similar to the average solution we obtained for faults in our domain 2 (compare with Fig. 10l). A normal fault solution (F3; Fig. 13) may reflect a rift basin located west of the Alpine Fault (Doser et al., 1999).

These similarities between the kinematic solutions we obtained for the Harrison–Kaipo fault zone and many of the earthquake focal mechanisms suggest that the faults we measured reflect deformation that occurred since 6.4 Ma when a decrease in the obliquity of plate convergence resulted in increased shortening and vertical uplift. Our calculated axes of shortening (*Z*) also are compatible with the azimuths of *P*-axes. Although *P*-axis azimuths cannot be related directly to principal stress axes, there is good agreement among the azimuths and the principal axes of shortening across the South Island (Anderson et al., 1993; Norris and Cooper, 1995; Moore et al., 2000). The shallow plunges of the *P*-axes shown in Fig. 13 indicate that their azimuths are well constrained. At least one *P*-axis azimuth in Fiordland (Event MI; Fig. 13) parallels the average axis of shortening we determined for the Harrison–Kaipo fault zone (Fig. 11b). Others from southern Fiordland parallel the *Z* axes in the reverse faults we measured (compare *Z*-axis orientation in Fig. 10l with *P*-axes of events L and 17 in Fig. 13). East of Fiordland, Norris et al. (1990) inferred NE directions of compression on NW-striking faults and NW directions of compression on NE-striking faults that are similar to our results for N-striking and NE-striking fault, respectively.

Despite the general agreement between average *P*-axis azimuths and the average orientation of shortening axes at the scale of the entire the South Island (Moore et al., 2000), the Fiordland data show a considerable amount of local variability. *P*-axes and *Z*-axes in Fiordland show variations in trend of up to 40° (Fig. 13). Moore et al. (2000) suggested that this variability, and even greater scatter in earthquake slip vector orientations, reflect pre-existing structures that locally control the orientation of faulting. The structural data and field relationships we observed strongly support this interpretation. We discuss how pre-existing structures locally controlled the orientation of faulting east of the Alpine Fault in the next section.

7.3. Fault mechanics and the effects of inherited structures

Mohr–Coulomb fracture criteria for confined compression (e.g., Price, 1966; Paterson, 1978) predict that conjugate dextral and sinistral faults form at angles of ~ 30° on either side of the maximum principal stress direction (*P*). Two-dimensional physical experiments of strike-slip faulting in homogeneous materials show that conjugate Riedel shears develop at angles of 15° and 75°, respectively, to the main fault in en echelon arrays (Riedel, 1929; Tchalenko, 1970; Harding, 1985; Naylor et al., 1986). North of Milford Sound the main traces of the Alpine, Pembroke and Harrison–Kaipo faults display average strikes ranging from 055° to 065° and are either approximately vertical or steeply southeast-dipping (80° SE). Consequently, the predicted orientations of Riedel shears are steep to vertical with strikes of 070–080° and 310–320° for dextral (R) and sinistral (R′) faults, respectively (Fig. 14a).

The sinistral-oblique and dextral-oblique fault populations we observed in Fiordland (Fig. 10) resemble

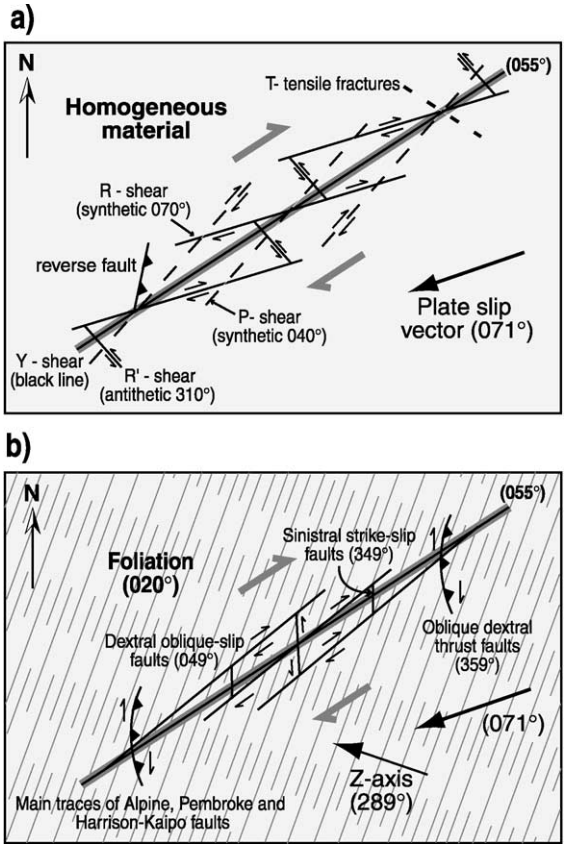

Fig. 14. Sketches showing fault geometries in the horizontal plane. (a) Geometry of en echelon faults predicted from physical experiments of strike-slip faulting. Orientations are based on the 055° strike of the Alpine Fault. Conjugate Riedel shears are synthetic (R) and antithetic (R′) to slip on the Alpine Fault. *P*-shears, *Y*-shears and tensile fractures (*T*) are also shown. (b) Observed fault geometry for the Harrison–Kaipo and Pembroke fault zones. Thin black lines are trace of vertical S_1 foliation (020°). Note that calculated axes of instantaneous strain (*Z*) are oriented clockwise from the plate slip vector. See text for discussion.

Riedel shears in the sense that the dextral set is synthetic (R) and the sinistral set is antithetic (R′) to the main traces of the Alpine, Pembroke and Harrison–Kaipo fault zones. However, the geometry and kinematics of the Fiordland faults deviate significantly from the predictions of experiments (Fig. 14). The angle between the average orientations of sinistral and dextral faults is 60°, however, the two sets form angles of 66° and 6° with respect to the 055° strikes of the Alpine and Pembroke faults, respectively. The dextral set also lies anticlockwise from the main trace of the Alpine Fault, contrary to the predictions from experimental data (compare Fig. 14a and b). Reverse faults do not occur at the predicted orientations (45° angles from the trace of the main fault). In addition, the fault geometry and kinematics fit patterns of triaxial not biaxial deformation. These patterns include mutually crosscutting fault sets involving both horizontal and vertical displacements. Three-dimensional kinematic heterogeneity is indicated by complex slip directions on differently oriented fault segments, including slickenline pitches ranging from 0° to 70–80° and variations in fault plane attitudes (Figs. 10 and 11a). These deviations offer important clues to the processes controlling deformation patterns east of Fiordland.

One possible explanation of the fault geometry we observed is that the faults rotated clockwise relative to the main NE-striking traces of the Pembroke and Harrison–Kaipo fault zones. Rotation of minor faults with respect to the main fault traces is expected for strike-slip styles of deformation (e.g., Tchalenko, 1970; Harding, 1985; Naylor et al., 1986). This type of rotation is different than that which has been proposed for the entire Fiordland Block between the Alpine Fault and the Moonlight Fault system (Walcott, 1998). In this latter case, the main traces of the Pembroke and Harrison–Kaipo faults also would have rotated. However, the acute angle between the dextral and sinistral fault sets is located in the wrong position relative to the main fault traces to be the result of rotated Riedel shears. Hence, this rotated Riedel shears model cannot explain the observed geometries.

Microstructural evidence showing a strong component of horizontal pure shear across the fault zone (Fig. 9B) helps explain some of the angular relationships we observed. Shortening across the fault zone most likely caused the different fault sets to rotate in opposite directions, thus producing angles that are larger than those predicted by experiments of strike-slip systems (Twiss and Moores, 1992, p. 173). However, the magnitude of the rotation needed to produce the observed angles of 66° and 6° with respect to the main fault trace is inconsistent with the low magnitudes of slip on the largest faults compared to estimates of the total strain. More than 60% of the total strain arising from plate motion (~ 70 km shortening according to Walcott, 1998) is required to produce significant deviations away from the

assumptions of instantaneous strain used in the fault-slip analysis (Cladouhos and Allmendinger, 1993). The faults also lie close to the main fault traces, which is a stable orientation that does not undergo large rotations (Norris and Cooper, 1995). We therefore conclude that fault rotation within a deformation field characterized by subhorizontal shortening across the fault zone can partly but not solely explain the observed angular relationships.

The characteristics of faulting we observed are very similar to patterns that typically form in mechanically anisotropic, previously deformed continental crust (Marrett and Allmendinger, 1990; Klepeis and Austin, 1997). Fracture experiments in anisotropic crust indicate that inherited weaknesses such as foliation planes strongly influence the orientation of fracture angles (Twiss and Moores, 1992). At angles of 15–60° between the maximum principal compressive stress (P) and inherited foliation planes, shear fractures develop approximately parallel to the foliation because shear strength is lower in these directions (Twiss and Moores, 1992, p. 178). This result explains why the Alpine Fault and Pembroke Fault reactivated the steep NE-striking (055°) foliation planes that define the Cretaceous Anita Shear Zone (Fig. 3). In these cases, the angle between the pre-existing basement anisotropy (055°) and the direction of maximum instantaneous shortening (289°) is 54°, a relationship which is predicted to result in the reactivation of the older planes of weakness (Twiss and Moores, 1992).

The geometry of faults in the Harrison–Kaipo fault zone exhibit a more complex relationship with pre-existing structures than the Alpine and Pembroke faults. The strike of the Cretaceous S_1 foliation (020°) east of the Anita Shear Zone is nearly perpendicular to the shortening direction (289°; Fig. 14b). This foliation remains steep for tens of kilometers south and away from the faulted parts of northern Fiordland although some localized tilting does occur. Hence, it is likely to reflect an originally steep geometry, much like the Anita Shear Zone that parallels the pre-late Cenozoic continental margin of western New Zealand. Experiments suggest that at angles between shortening directions and inherited foliation planes that are greater than 60°, pre-existing planes of weakness still have a strong influence on the fracture plane orientation (Twiss and Moores, 1992, p. 178). However, in these cases, instead of reactivating old planes of weakness fractures develop across foliation planes. Because of the nearly orthogonal relationship between the Z-axis and the S_1 foliation (Fig. 14b), little to no resolved shear stress occurs on the old foliation planes so reactivation does not occur. These relationships explain why the main traces of the Harrison–Kaipo Fault zone cut obliquely across the S_1 foliation instead of reactivating them (Fig. 14b).

On the basis of these relationships we conclude that pre-Cenozoic structures influenced the heterogeneous geometry of Late Tertiary faults in northern Fiordland. This interpretation is consistent with other regional structural patterns. Offshore geophysical data also suggest that Cretaceous and older discontinuities controlled Eocene and younger deformation patterns, including the Alpine Fault, south west of Fiordland (Lebrun et al., 2000; Sutherland et al., 2000). Structural evidence (e.g., Norris et al., 1990) also suggests that Cretaceous normal faults south and east of Fiordland (Fig. 1b) were reactivated as oblique-slip faults during the Late Tertiary. We add the point that the orientations of these and other pre-Cenozoic structures with respect to the regional axes of shortening explain the variability of faulting and slip vectors that result from regional transpression.

7.4. Implications for kinematic partitioning

A comparison of kinematic patterns northeast and southwest of Milford Sound indicates that an unusual style and degree of strike-slip partitioning occurs in northernmost Fiordland. Along the central segments of the Alpine Fault north of Fiordland, Norris and Cooper (1995) described a partitioning of oblique-reverse slip on moderately ESE-dipping surfaces that strike between 020° and 050° and dextral slip on steep surfaces that strike between 065° and 090°. In contrast, slip on the southernmost onshore segment of the Alpine Fault north of Milford Sound is nearly horizontal and occurs on subvertical surfaces (Berryman et al., 1992; Sutherland and Norris, 1995; Norris and Cooper, 2001). These observations and the oblique-reverse slip that occurs away from the Alpine Fault in the Milford Sound region indicates that the degree of strike-slip partitioning in northernmost Fiordland is higher than that observed farther north.

In the central part of the South Island, Cox and Findlay (1995) described an oblique-reverse fault

zone, called the Main Divide fault zone, that formed east of the Alpine Fault during the late Cenozoic. This fault zone displays a stepped oblique-reverse and strike-slip segmentation that is similar in style and location to the Harrison–Kaipo fault zone. However, the thrust segments of the Main Divide Fault Zone dip 40–60° to the northwest, creating an antithetic back-thrust in the hanging wall of the Alpine Fault. In contrast, the Harrison–Kaipo thrust segments dip to the east. These observations indicate that the geometry of oblique-reverse faults in northernmost Fiordland are also different than those observed in central segments of the South Island.

South of Milford Sound, where the Alpine Fault is located offshore, earthquake data indicate that the relative magnitude of the reverse component of displacement accommodated by the Alpine Fault gradually increases to the southwest (compare events C8, MI, and 27 in Fig. 13). Moore et al. (2000) noted that earthquakes in this region (such as events MI, JB, L, C4, 17 and 27; Fig. 13) display larger convergent components than predicted by the Nuvel 1a relative plate motion vector. This result implies that a missing component of strike-slip motion is accommodated to the east of the Alpine Fault south of Milford Sound (Moore et al., 2000). The southern segment of the Fiordland Boundary Fault likely accommodates some of this missing strike-slip motion, as indicated by the solution to earthquake event E (Fig. 13). This result also suggests that the Harrison–Kaipo and Hollyford faults form a transfer zone that links oblique-slip displacements northeast of Fiordland with dextral strike-slip on Moonlight–Fiordland Boundary fault zone to the southeast.

Just as the Fiordland Boundary Fault appears to accommodate the missing strike-slip component along the plate boundary in southern Fiordland, the near horizontal slip on the Alpine Fault near Milford Sound implies that a missing component of thrust motion must be accommodated elsewhere. We suggest that the oblique-reverse faults located in northeast Fiordland such as those in the Harrison–Kaipo fault zone accommodate this missing thrust component. The concentration of shortening in northeastern Fiordland appears to be enhanced by the interaction between Fiordland crust, which is moving northward, and the thick lithospheric root of the Southern Alps (Furlong et al., 2001). Furlong et al. (2001) suggested that this root acts as a buttress that influences the kinematics of transpression in this region and the geometry of the Australian plate beneath Fiordland. Norris and Turnbull (1993) also suggested that the initiation of strike-slip motion on the Moonlight Fault system in the Miocene resulted in crustal shortening along the northeast edge of Fiordland. We suggest that this focusing of shortening to northeast Fiordland helps explain why the Alpine Fault north of Milford Sound accommodates more strike-slip motion than predicted by the Nuvel-1a relative plate motion vector.

The partitioning of strike-slip motion on the Alpine Fault near Milford Sound may also be enhanced by its near vertical orientation in this region. Rattenbury (1986) and Walcott (1998) suggested that the development of thrust splays east of the central segments of the Alpine Fault originated from a shallowing of the dip of the fault from near vertical to 50° at about 6.4 Ma when the angle of oblique convergence increased. These changes appear to have initiated the oblique-slip motion observed on most segments of the Alpine Fault (Walcott, 1998). In northern Fiordland, we showed that the orientation of the Anita Shear Zone (and the pre-late Cenozoic continental margin) with respect to shortening (Z) axes promoted the reactivation of this mechanical weakness rather than the formation of new fractures across it. We suggest that the mechanical effect of this basement anisotropy helped maintain the steep orientation of the Alpine Fault in the Milford Sound region after 6.4 Ma. In this sense, a combination of steep basement anisotropies which controlled the orientation of the Alpine Fault and the focusing of thrust motion in northernmost Fiordland resulted in the unusually high degree of kinematic partitioning near Milford Sound.

8. Conclusions

Structural, kinematic and preliminary geochronologic data show that 6.5–7.0 km of reverse and oblique-reverse displacements were partitioned into fault zones within and at the boundaries of Fiordland's high-P granulite belt. Conventional K–Ar ages from mylonitic, upper greenschist facies segments of the Pembroke and Alpine fault zones suggest that dextral strike-slip faulting and transpression likely began in the

latest Oligocene–early Miocene. On the basis of cross-cutting relationships and the youngest ages of the exhumed mylonites, the brittle faults we measured are younger than 7–9 Ma. The curved segments of the Harrison–Kaipo and Pembroke faults create curved, branching geometries that include subhorizontal detachments in profile. These faults dissect the granulite belt into fault-bounded wedges that have been shuffled vertically, creating both reverse and normal separations across steep fault planes. Fault segments that parallel the NE strike of the Alpine Fault accommodated a smaller amount of oblique-reverse displacements and more strike-slip displacements. Segments that strike N, NNW and WNW accommodated reverse displacements. High-*P* granulites of the Arthur River Complex form one of these wedges that has been squeezed up vertically between steep segments of the Harrison–Kaipo and Pembroke faults. The Darran Complex forms another wedge that has been thrust obliquely over the granulites along the northern sections of the Harrison–Kaipo fault zone. Reverse faulting coupled with erosion led to 3.0–5.5 km of exhumation resulting in exposure of the upper greenschist facies mylonites. Variations in the geometry of steep, pre-Cenozoic basement anisotropies controlled the unusual orientation of the Alpine Fault and the geometry of faults located to the southeast in the Milford Sound region. The mechanical effects of inherited structures and a focusing of contractional deformation at the northeastern margin of Fiordland resulted in the unusually high degree of strike-slip partitioning that occurs near Milford Sound.

Acknowledgements

Funding to support this work was provided by Australian Research Council funding to KAK and GLC (ARC-A10009053), National Science Foundation funding to KAK (EAR-0087323), funding to ALC from the Geological Society of America Harold T. Stearns Fellowship Award (GSA-6624-00), and a University of Vermont Research grant. We thank Nathan Daczko, Nick Mortimer and Ian Turnbull of the IGNS, Dunedin for many helpful discussions and assistance, and Allan Munn of the Department of Land Conservation in Te Anau for permission to visit and sample localities in the Fiordland National Park. Thanks go to J.A. Stevenson and A. Papadakis for their assistance in the field. KAK thanks Simon Nathan of the IGNS, Wellington for helping us obtain and process DTM data and G. Mora and R. Sutherland for discussions on Fiordland geology. We also thank J.F. Lebrun for his careful review and K. Furlong for comments on the original mansucript.

Appendix A. Analytical procedures for isotopic analyses

Potassium content was determined by atomic absorption (Varian AA 20). The pooled error of duplicate K determinations on samples and standards is better than 3%. The error for argon analyses is below 1.50% and the $^{40}Ar/^{36}Ar$ value for air shots averaged 294.39 ± 0.201 (2σ, $n=5$). Ar isotopic determinations were performed according to procedures described by Bonhomme et al. (1975). Samples were pre-heated under vacuum at 80 °C for several hours to reduce the amount of atmospheric Ar adsorbed onto the mineral surfaces during sample handling. Argon was extracted from the separated mineral fractions by fusing samples within a vacuum line serviced by an on-line ^{38}Ar spike pipette. The isotopic composition of the spiked Ar was measured with a high sensitivity VG3600 mass spectrometer. The ^{38}Ar spike was calibrated against international standard biotite GA1550 (McDougall and Roksandic, 1974). After fusion of the sample in a low blank Heine resistance furnace, the released gases were purified with a Cu_2O getter followed by two TiO_2 getters. Blanks for the extraction line and mass spectrometer and the mass discrimination factor were determined by airshots. Five airshot values were measured and six international standard references were used including GA1550: McDougall and Roksandic (1974); GL-O and LP 6: Odin et al. (1982); HD-B1: Hess and Lippolt (1994).

References

Anderson, H., Webb, T., Jackson, J., 1993. Focal mechanisms of large earthquakes in the South Island of New Zealand: implications for the accommodation of Pacific–Australia plate motion. Geophys J. Int. 115, 1032–1054.

Berryman, K.R., Beanland, S., Cooper, A.F., Cutten, H.N., Norris, R.J., Wood, P.R., 1992. The Alpine Fault, New Zealand: varia-

tion in Quaternary structural style and geomorphic expression. Ann. Tecton. 6, 126–163.

Blattner, P., 1976. Replacement of hornblende by garnet in granulite facies assemblages near Milford Sound, New Zealand. Contrib. Mineral. Petrol. 55, 181–190.

Blattner, P., 1978. Geology of crystalline basement between Milford Sound and the Hollyford Valley, New Zealand. N.Z. J. Geol. Geophys. 21, 33–47.

Blattner, P., 1991. The North Fiordland transcurrent convergence. N.Z. J. Geol. Geophys. 34, 543–553.

Bonhomme, M.G., Thuizat, R., Pinault, Y., Clauer, N., Wendling, R., Winkler, R., 1975. Méthode de datation potassium–argon. Appareillage et Technique, Notes technique de l'Institut de Géologie, No. 3, Université Louis Pasteur, Strasbourg, p. 53.

Bradshaw, J.Y., 1989. Origin and metamorphic history of an Early Cretaceous polybaric granulite terrain, Fiordland, southwest New Zealand. Contrib. Mineral. Petrol. 103, 346–360.

Bradshaw, J.Y., 1990. Geology of crystalline rocks of northern Fiordland: details of the granulite facies Western Fiordland Orthogneiss and associated rock units. N.Z. J. Geol. Geophys. 33, 465–484.

Braun, J., Beaumont, C., 1995. Three-dimensional numerical experiments if strain partitioning at oblique plate boundaries: implications for the contrasting styles in the southern Coast Ranges, California and central South Island, New Zealand. J. Geophys. Res. 100, 18059–18074.

Brown, E.H., 1996. High-pressure metamorphism caused by magma loading in Fiordland, New Zealand. J. Metamorph. Pet. 14, 441–452.

Bull, W.B., Cooper, A.F., 1986. Uplifted marine terraces along the Alpine Fault, New Zealand. Science 240, 804–805.

Butler, R.W.H., Spencer, S., Griffiths, H.M., 1998. The structural response to evolving plate kinematics during transpression: evolution of the Lebanese restraining bend of the Dead Sea Transform. In: Holdsworth, R.E., Strachan, R.A., Dewey, J.F. (Eds.), Continental transpressional and transtensional tectonics. Geological Society of London Special Publications, vol. 135, pp. 81–106.

Chase, C.G., 1978. Plate kinematics: the Americas, East Africa and the rest of the world. Earth Planet. Sci. Lett. 37, 355–368.

Cladouhos, T.T., Allmendinger, R.W., 1993. Finite strain and rotation from fault slip data. J. Struct. Geol. 15, 771–784.

Clarke, G.L., Klepeis, K.A., Dazcko, N.R., 2000. Cretaceous high-*P* granulites at Milford Sound, New Zealand: metamorphic history and emplacement in a convergent margin setting. J. Metamorph. Geol. 18, 359–374.

Coombs, D.S., Landis, C.A., 1985. Permian–Jurrasic of Southland and South Otago. Geol. Soc. N.Z. Misc. Publ. 33A, 153–166.

Cooper, A.F., Barreiro, B.A., Kimbrough, D.L., Mattinson, J.M., 1987. Lamprophyre dike intrusion and the age of the Alpine fault, New Zealand. Geology 15, 941–944.

Cox, S.C., Findlay, R.H., 1995. The Main Divide fault zone and its role in formation of the Southern Alps, New Zealand. N.Z. J. Geol. Geophys. 38, 489–499.

Daczko, N.R., Klepeis, K.A., Clarke, G.L., 2001. Evidence of Early Cretaceous collisional-style orogenesis in northern Fiordland, New Zealand and its effects on the evolution of the lower crust. J. Struct. Geol. 23, 693–713.

Davey, F.J., Smith, E.G.C., 1983. The tectonic setting of the Fiordland region, south-west New Zealand. Geophys. J. R. Astron. Soc. 72, 23–38.

Davids, C., Gibson, G.M., 2001. Stepwise cooling and exhumation of a granulite terrane in Fiordland, New Zealand. Earth Systems Processes Programmes with abstracts, 24–28 June. Edinburgh, Scotland, p. 121.

DeMets, C., Gordon, R.G., Argus, D.F., Stein, S., 1994. Current plate motions. Geophys. J. Int. 101, 425–478.

Dockrill, B.R., 2000. The decompressional history of Northern Fiordland and its relationship to a Cretaceous–Tertiary crustal scale shear zone. Unpublished BSc (Honours) thesis, University of Sydney, Sydney.

Doser, D.I., Webb, T.H., Maunder, D.E., 1999. Source parameters of large (1918–1962) earthquakes, South Island, New Zealand. Geophys. J. Int. 139, 769–794.

Fossen, H., Tikoff, B., 1998. Extended models of transpression and transtension, and application to tectonic settings. In: Holdsworth, R.E., Strachan, R.A., Dewey, J.F. (Eds.), Continental Transpressional and Transtensional Tectonics. Geol. Soc. London Spec. Publ., vol. 135, pp. 15–33.

Furlong, K.P., Malservisi, R., Anderson, H., 2001. Initiation of Subduction in a Complex Transpressional Regime, Fiordland, New Zealand. EOS Trans. AGU 82 (47) (Fall Meet. Suppl., Abstract T41F-03).

Gaina, C., Müller, D.R., Royer, J.-Y., Stock, J., Hardebeck, J., Symonds, P., 1998. The tectonic history of the Tasman Sea: a puzzle with thirteen pieces. J. Geophys. Res. 103, 12413–12433.

Geary, E.E., Paterson, S.R., 1990. Geochemical characteristics of metaigneous rocks near the Alpine Fault, New Zealand. Geol. Soc. Amer. Abstr. Prog. 22 (7), 163.

Gibson, G.M., 1990. Uplift and exhumation of middle and lower crustal rocks in an extensional tectonic setting, Fiordland, New Zealand. In: Fountain, M.H., Salisbury, D.M. (Eds.), Exposed Cross-Sections of the Continental Crust. Kluwer Academic Publishing, Dordrecht, pp. 71–101.

Gibson, G.M., Ireland, T.R., 1995. Granulite formation during continental extension in Fiordland. Nature 375, 479–482.

Gibson, G.M., McDougall, I., Ireland, T.R., 1988. Age constraints on metamorphism and the development of a metamorphic core complex in Fiordland, southern New Zealand. Geology 16, 405–408.

Harding, T.P., 1985. Seismic characteristics and identification of negative flower structures, positive flower structures and positive structural inversion. Bull. Am. Assoc. Pet. Geol. 69, 582–600.

Hervé, F., 1994. The southern Andes between 39° and 44°S latitude: the geological signature of a transpressive tectonic regime related to a magmatic arc. In: Reutter, K.J., Scheuber, E., Wigger, P.J. (Eds.), Tectonics of the Southern Central Andes. Springer Verlag, New York, pp. 243–248.

Hess, J.C., Lippolt, H.J., 1994. Compilation of K–Ar measurements on HD-B1, standard biotite. In: Odin, G.S. (Ed.), Phanerozoic Time Scale. Bull. Lias. Inform., IUGS subcom. Geochron., vol. 12, pp. 19–23. Paris.

Hill, E.J., 1995. A deep crustal shear zone exposed in western Fiordland, New Zealand. Tectonics 14, 1172–1181.

Hollis, J.A., 1996. The Pressure–Temperature history of Cretaceous granulites in Milford Sound, New Zealand. Unpublished BSc (Honours) thesis, University of Sydney, Sydney.

Holm, D.K., Norris, R.J., Craw, D., 1989. Brittle and ductile deformation in a zone of rapid uplift: central southern Alps, New Zealand. Tectonics 8, 153–168.

Ireland, T.R., Gibson, G.M., 1998. SHRIMP monazite and zircon geochronology of high-grade metamorphism in New Zealand. J. Metamorph. Geol. 16, 149–167.

Jiang, D., Lin, S., Williams, P.F., 2001. Deformation path in high-strain zones, with reference to slip partitioning in transpressional plate-boundary regions. J. Struct. Geol. 23, 991–1005.

Kamb, W.B., 1959. Petrofabric observations from Blue Glacier, Washington, in relation to theory and experiment. J. Geophys. Res. 64, 1908–1909.

Kimbrough, D.L., Tulloch, A.J., Coombs, D.S., Landis, C.A., Johnston, M.R., Mattinson, J.M., 1994. Uranium–lead zircon ages from the Median Tectonic Zone, New Zealand. N.Z. J. Geol. Geophys. 37, 393–419.

Klepeis, K.A., Austin, J.A., 1997. Contrasting styles of superposed deformation in the southernmost Andes. Tectonics 16, 755–776.

Klepeis, K.A., Dazcko, N.R., Clarke, G.L., 1999. Kinematic vorticity and tectonic significance of superposed mylonites in a major lower crustal shear zone, northern Fiordland, New Zealand. J. Struct. Geol. 21, 1385–1405.

Koons, P.O., 1978. Aspects of the geology of the southern Darran Mountains. N.Z. Geol. Sur. Rep. G26.

Koons, P.O., 1994. Three-dimensional critical wedges: tectonics and topography in oblique collisionalorogens. J. Geophys. Res. 99, 12301–12315.

Koons, P.O., Henderson, C.M., 1995. Geodetic analysis of model oblique collision and comparison to the Southern Alps of New Zealand. N.Z. J. Geol. Geophys. 38, 545–552.

Lamarche, G., Collot, J.-Y., Wood, R.A., Sosson, M., Sutherland, R., Delteil, J., 1997. The Oligocene–Miocene Pacific–Australia plate boundary, south of New Zealand: evolution from oceanic spreading to strike-slip faulting. Earth Planet. Sci. Lett. 148, 129–139.

Landis, C.A., 1980. Little Ben Sandstone, Maitai Group (Permian): nature and extent in the Hollyford region, South Island, New Zealand. N.Z. J. Geol. Geophys. 23, 551–567.

Lebrun, J.-F., Lamarche, G., Collot, J.-Y., Delteil, J., 2000. Abrupt strike-slip fault to subduction transition: the Alpine Fault–Puysegur trench connection, New Zealand. Tectonics 19 (4), 688–706.

Little, T.A., 1996. Faulting-related displacement gradients and strain adjacent to the Awatere strike-slip fault in New Zealand. J. Struct. Geol. 18, 321–340.

Marrett, R.A., Allmendinger, R.W., 1990. Kinematic analysis of fault-slip data. J. Struct. Geol. 12, 973–986.

Mattinson, J.L., Kimbrough, D.L., Bradshaw, J.Y., 1986. Western Fiordland orthogneiss: early cretaceous arc magmatism and granulite facies metamorphism, New Zealand. Contrib. Mineral. Petrol. 92, 383–392.

McCaffrey, R., 1992. Oblique plate convergence, slip vectors, and forearc deformation. J. Geophys. Res. 97, 8905–8915.

McCulloch, M.T., Bradshaw, J.Y., Taylor, S.R., 1987. Sm–Nd and Rb–Sr isotopic and geochemical systematics in Phanerozoic granulites from Fiordland, Southwest New Zealand. Contrib. Mineral. Petrol. 97, 183–195.

McDougall, I., Roksandic, Z., 1974. Total fusion $^{40}Ar/^{39}Ar$ ages using HIFAR reactor. J. Geol. Soc. Aust. 21, 81–89.

Molnar, P., 1983. Average regional strain due to slip on numerous faults of different orientations. J. Geophys. Res. 88, 6430–6432.

Moore, M.A., Anderson, H.J., Pearson, C., 2000. Seismic and geodetic constraints on plate boundary deformation across the northern Macquarie Ridge and southern South Island of New Zealand. Geophys. J. Int. 143 (3), 847–880.

Mortimer, N., Tulloch, A.J., Spark, R., Walker, N., Ladley, E., Kimbrough, D.L., Allibone, A.H., 1999. Overview of the Median Batholith, New Zealand: a new interpretation of the geology of the Median Tectonic Zone and adjacent rocks. J. Afr. Earth Sci. 29, 257–268.

Mount, V.S., Suppe, J., 1987. State of stress near the San Andreas fault: implications for wrench tectonics. Geology 15, 1143–1146.

Muir, R.J., Weaver, S.D., Bradshaw, J.D., Eby, G.N., Evans, J.A., 1995. The Cretaceous Separation Point batholith, New Zealand: granitoid magmas formed by melting of mafic lithosphere. J. Geol. Soc. Lond. 152, 689–701.

Muir, R.J., Ireland, T.R., Weaver, S.D., Bradshaw, J.D., Evans, J.A., Eby, G.N., Shelley, D., 1998. Geochronology and geochemistry of a Mesozoic magmatic arc system, Fiordland, New Zealand. J. Geol. Soc. Lond. 155, 1037–1053.

Nathan, S., Thurlow, C., Warnes, P., Zucchetto, R., 2000. Geochronology database for New Zealand rocks: 1961–1999, 2nd ed. Inst. Geol. Nuc. Sci. Rep., vol. 11, p. 51.

Naylor, M.A., Mandland, G., Sijpesteijn, C.H.K., 1986. Fault geometries in basement-induced wrench faulting under different initial stress states. J. Struct. Geol. 8, 737–752.

Norris, R.J., Carter, R.M., 1980. Offshore sedimentary basins at the southern end of the Alpine Fault, New Zealand. In: Balance, P.F., Reading, H.G. (Eds.), Sedimentation and Oblique-Slip Mobile Zones. Spec. Publ. Int. Ass. Sediment., vol. 4, pp. 237–265.

Norris, R.J., Carter, R.M., 1982. Fault-bounded blocks and their role in localising sedimentation and deformation adjacent to the Alpine Fault, southern New Zealand. Tectonophysics 87, 11–23.

Norris, R.J., Cooper, A.F., 1995. Origin of small-scale segmentation and transpressional thrusting along the Alpine fault, New Zealand. Geol. Soc. Am. Bull. 107, 231–240.

Norris, R.J., Cooper, A.F., 2001. Late Quaternary slip rates and slip partitioning on the Alpine Fault, New Zealand. J. Struct. Geol. 23, 507–520.

Norris, R.J., Turnbull, I.M., 1993. Cenozoic basins adjacent to an evolving transform plate boundary, southwest New Zealand. In: Ballance, P.F. (Ed.), South Pacific Sedimentary Basins. Elsevier, New York, pp. 251–270.

Norris, R.J., Carter, R.M., Turnbull, I.M., 1978. Cainozoic sedimentation in basins adjacent to a major continental transform boundary in southern New Zealand. J. Geol. Soc. (Lond.) 135, 191–205.

Norris, R.J., Koons, P.O., Cooper, A.F., 1990. The obliquely-convergent plate boundary in the South Island of New Zealand: implications for ancient collision zones. J. Struct. Geol. 12, 715–725.

Odin, G.S., et al., 1982. Interlaboratory standards for dating purposes. In: Odin, G.S. (Ed.), Numerical Dating in Stratigraphy, Part 1. Wiley, Chichester, pp. 123–148.

Oliver, G.J.H., 1980. Geology of the granulite and amphibolite facies gneisses of Doubtful Sound, Fiordland, New Zealand. N.Z. J. Geol. Geophys. 1, 27–41.

Oliver, G.J.H., 1990. An exposed cross-section of continental crust, Doubtful Sound, Fiordland, New Zealand; Geophysical and geological setting. In: Salisbury, M.H., Fountain, D.M. (Eds.), Exposed Cross-Sections of the Continental Crust. Kluwer Academic Publishing, Netherlands, pp. 43–69.

Oliver, G.J.H., Coggon, J.H., 1979. Crustal structure of Fiordland, New Zealand. Tectonophysics 54, 253–292.

Passchier, C.W., Trouw, R.A.J., 1996. Microtectonics. Springer Verlag, Berlin, p. 289.

Paterson, M.S., 1978. Experimental Rock Deformation: The Brittle Field. Springer Verlag, New York, p. 254.

Price, N.J., 1966. Fault and Joint Development in Brittle and Semi-Brittle Rock. Pergamon, New York, p. 176.

Rattenbury, M., 1986. Late low-angle thrusting and the Alpine Fault, central Westland, New Zealand. N.Z. J. Geol. Geophys. 29, 437–446.

Rattenbury, M., 1991. The Fraser Complex; high-grade metamorphic, igneous and mylonitic rocks in central Westland, New Zealand. N.Z. J. Geol. Geophys. 34, 23–33.

Riedel, W., 1929. Zur Mechanik geologischer Brucherscheinungen. Centralbl. Min. Geol., 354–368.

Simpson, C., De Paor, D.G., 1993. Strain and kinematic analysis in general shear zones. J. Struct. Geol. 15, 1–20.

Steiger, R.H., Jäger, E., 1977. Subcommission on geochronology: convention on the use of decay constants in geo- and cosmochronology. Earth Planet. Sci. Lett. 36, 359–362.

Sutherland, R., 1994. Displacement since the Pliocene along the southern section of the Alpine fault, New Zealand. Geology 22, 327–330.

Sutherland, R., 1995. The Australia–Pacific boundary and Cenezoic plate motions in the SW Pacific: some constraints from Geosat data. Tectonics 14, 819–831.

Sutherland, R., 1996. Transpressional development of the Australia–Pacific boundary through southern South Island, New Zealand: constraints from Miocene–Pliocene sediments, Waiho-1 borehole, South Westland. N.Z. J. Geol. Geophys. 39, 251–264.

Sutherland, R., Norris, R.J., 1995. Late Quaternary displacement rate, paleoseismicity, and geomorphic evolution of the Alpine Fault: evidence from Hokuri Creek, South Westland, New Zealand. N.Z. J. Geol. Geophys. 38, 419–430.

Sutherland, R., Davey, F., Beavan, J., 2000. Plate boundary deformation in South Island, New Zealand, is related to inherited lithospheric structure. Earth Planet. Sci. Lett. 177, 141–151.

Sylvester, A.G., 1988. Strike-slip faults. Geol. Soc. Am. Bul. 100, 1666–1703.

Tchalenko, J.S., 1970. Similarities between shear zones of different magnitudes. Geol. Soc. Am. Bull. 81, 1625–1640.

Teyssier, C., Tikoff, B., Markley, M., 1995. Oblique plate motion and continental tectonics. Geology 23, 447–450.

Tulloch, A.J., Kimbrough, D.L., 1989. The Paparoa metamorphic core complex, New Zealand: Cretaceous extension associated with fragmentation of the Pacific margin of Gondwana. Tectonics 8, 1217–1234.

Tulloch, A.J., Ireland, T.R., Walker, N.W., Kimbrough, D.L., 2000. U–Pb zircon ages from the Milford Orthogneiss, Milford Sound, northern Fiorland: Paleozoic igneous emplacement and Early Cretaceous metamorphism. Inst. Geol. Nucl. Sci. Rep. 6, 17.

Twiss, R.J., Moores, E.M., 1992. Structural Geology. Freeman, New York, p. 532.

Walcott, R.I., 1979. Plate motions and shear strain rates in the vicinity of the Southern Alps. In: Walcott, R.I., Creswell, M.M. (Eds.), The Origin of the Southern Alps. Roy. Soc. N.Z. Bull., vol. 18, pp. 5–12.

Walcott, R.I., 1998. Modes of oblique compression: Late Cenozoic tectonics of the South Island of New Zealand. Rev. Geophys. 36, 1–26.

Wandres, A.M., Weaver, S.D., Shelley, D., Bradshaw, J.D., 1998. Change from calc-alkaline to adakitic magmatism recorded in the early Cretaceous Darran Complex, Fiordland, New Zealand. N.Z. J. Geol. Geophys. 41, 1–14.

Weissel, J.K., Hayes, D.E., Herron, E.M., 1977. Plate tectonics synthesis: the displacements between Australia, New Zealand, and Antarctic since the late Cretaceous. Mar. Geol. 25, 231–277.

Wellman, H.W., 1953. Data for the study of recent and late Pleistocene faulting in the South Island of New Zealand. N.Z. J. Sci. Technol. B 34, 270–288.

Wood, B.L., 1962. New Zealand Geological Survey Map 1:250 000, Sheet 22. Wakatipu, First Edition.

Wood, B.L., 1972. Metamorphosed ultramafites and associated formations near Milford Sound, New Zealand. N.Z. J. Geol. Geophys. 15, 88–128.

Woodcock, N.H., Fischer, M., 1986. Strike-slip duplexes. J. Struct. Geol. 8, 725–735.